A viral protein utilizes the NDP52/CALCOCO2 selective autophagy receptor to disassemble processing bodies

Carolyn-Ann Robinson[1,2,3,4], Gillian K. Singh[1,4], Elizabeth L. Castle[1], Bre Q. Boudreau[1], Jennifer A. Corcoran[1,2,3,5]

[1]Department of Microbiology & Immunology, Dalhousie University, Halifax, NS, Canada

[2]Microbiology, Immunology & Infectious Diseases Department, University of Calgary, Calgary, AB, Canada.

[3]Charbonneau Cancer Research Institute, University of Calgary, Calgary, AB, Canada.

[4]Equal Contribution

[5]Corresponding Author

Abstract

Selective autophagy receptors contribute to host defence by targeting intracellular microbes for degradation and fine-tuning inflammatory processes by directing the degradation of macromolecular immune signaling platforms. Processing bodies (PBs) are cytoplasmic ribonucleoprotein granules that control inflammation by silencing and/or degrading labile messenger RNAs (mRNAs) that encode inflammatory mediator proteins. PBs often disassemble in response to virus infection, which correlates with increased synthesis of inflammatory mediator proteins; however, PB disassembly mechanisms remain largely obscure. Here, we demonstrate that the Kaposi's sarcoma-associated herpesvirus (KSHV) KapB protein increases the synthesis of inflammatory mediators by driving autophagy and triggering PB disassembly. This could be prevented by silencing of *Atg5* or the selective autophagy receptor *NDP52/CALCOCO2*, whereas silencing other selective autophagy receptors *p62* and *OPTN* had no effect on PB turnover or inflammatory mediator synthesis. These studies reveal a new role for NDP52 in regulating PB turnover in response to viral infection.

Keywords: processing bodies/Kaposi's sarcoma-associated herpesvirus/NDP52/selective autophagy/cytokine mRNA

Introduction

Macroautophagy, hereafter referred to as autophagy, is a process during which bulk cytoplasmic material is targeted for lysosomal degradation (Morishita & Mizushima, 2019; Levine *et al*, 2008). This process begins with the formation of a phagophore that elongates and encloses a portion of the cytoplasm to form a double-membrane specialized organelle, the autophagosome (Klionsky *et al*, 2012; Lamb *et al*, 2013). Essential for autophagosome expansion is the C-terminal lipidation of the microtubule associated protein 1 light chain 3 (LC3) protein, known as LC3-II, that allows it to invade the inner and outer autophagosome membranes (Klionsky *et al*, 2012). The outer membrane of the autophagosome then fuses with a lysosome to form an autolysosome, leading to degradation of the enclosed cargo along with the autophagosomal membrane and autophagy regulatory proteins including LC3-II.

Autophagy is a dynamic process, under basal conditions, autophagic activity ensures the continuous recycling of cellular resources and the clearance of damaged macromolecular complexes and organelles, maintaining cellular homeostasis and acting as an intracellular quality control system (Green *et al*, 2011). Various changes to the cellular microenvironment, including nutrient scarcity, hypoxia, and endoplasmic reticulum (ER) stress can drive autophagy and cause degradation of damaged organelles (e.g mitochondria, peroxisomes), protein complexes (e.g. focal adhesion complexes) or other targets in a more selective manner (Maiuri & Kroemer, 2015; Mizushima *et al*, 2010; Balgi *et al*, 2009; Kenific *et al*, 2016; Sargsyan *et al*, 2015; Tripathi *et al*, 2016; Dunn *et al*, 2005; Yao & Klionsky, 2016). In such cases, before the cargo is engulfed by the autophagosome it is selected for degradation by direct binding to LC3 or indirect targeting to LC3 via molecular bridges termed selective autophagy receptors (SARs). Some of the best characterized SARs include p62/SQSTM1, valosin containing protein (VCP), optineurin (OPTN), neighbor of BRCA1 gene 1 (NBR1) and nuclear dot protein 52 (NDP52/calcium binding and coiled-coil domain protein, CALCOCO2) (Zaffagnini & Martens, 2016). OPTN, p62, NDP52, and NBR1 are members of the sequestosome-like family and contain several conserved motifs including a LC3-interacting region (LIR), a domain that permits receptor multimerization and a ubiquitin-binding domain (UBD) (Ichimura *et al*, 2008; Noda *et al*, 2010; Birgisdottir *et al*, 2013; Noda *et al*, 2008). The selection of cargo for degradation can occur in a ubiquitin-dependent or -independent manner, although ubiquitin modification is believed to more efficiently recruit cargo to autophagosomes (Rogov *et al*, 2014). SARs play important

homeostatic roles maintaining, and at times magnifying, the turnover of mitochondria (mitophagy), peroxisomes (pexophagy) or protein complexes and this regulation facilitates cell survival in response to environmental changes (Maiuri & Kroemer, 2015; Mizushima *et al*, 2010; Balgi *et al*, 2009; Kenific *et al*, 2016; Sargsyan *et al*, 2015; Tripathi *et al*, 2016; Dunn *et al*, 2005; Yao & Klionsky, 2016).

Autophagy can also select, sequester and degrade invading pathogens such as viruses in a process called xenophagy and many viruses disarm this process (Orvedahl & Levine, 2008). Moreover, emerging evidence shows that selective autophagy receptors play important roles in fine-tuning innate immune responses by targeting key signaling platforms for degradation (Chen *et al*, 2016; Du *et al*, 2018; Jin *et al*, 2017; Prabakaran *et al*, 2018; Yang *et al*, 2017; He *et al*, 2019). For example, NDP52 is required for the autophagic degradation of interferon regulatory factor 3 (IRF3) and mitochondrial antiviral signaling protein (MAVS), which supports the resolution phase of type I interferon signaling (Wu *et al*, 2020) (Seth *et al*, 2005; Jin *et al*, 2017). Both pro and antiviral roles have been attributed to selective autophagy receptors (Sumpter & Levine, 2011; Ahmad *et al*, 2018) and viruses can both enhance or limit SAR function accordingly, promoting their replication (Mohamud *et al*, 2019). However, much remains to be discovered about the interplay between selective autophagy, control of innate immune responses, and virus infection (Sumpter & Levine, 2011; Levine *et al*, 2011).

Kaposi's sarcoma-associated herpesvirus (KSHV) is the infectious cause of the endothelial cell cancer, Kaposi's sarcoma (KS) and two B-cell malignancies (Cesarman *et al*, 1995; Chang *et al*, 1994; Soulier *et al*, 1995). KS lesions are typified by aberrant angiogenesis, tortuous leaky blood vessels, and inflammation; KS tumours are rich in inflammatory cytokines such as tumour necrosis factor (TNF), interleukins -1alpha, -1beta and -6 (IL-1α, IL-1β, IL-6), C-X-C Motif Chemokine Ligand 8 (CXCL8), interferon-gamma 2 (INF-γ), vascular endothelial growth factor (VEGF), cyclooxygenase-2 (COX-2) and granulocyte-macrophage colony-stimulating factor (GM-CSF) (Ensoli *et al*, 2010; Ensoli & Stürzl, 1998; Lane *et al*, 2002; Miles *et al*, 1990; Riva *et al*, 2010; Sadagopan *et al*, 2007; Salahuddin *et al*, 1988). Infection with KSHV has two forms, a latent and a lytic phase; it is the latent phase that predominates in KS tumours (Decker *et al*, 1996; Staskus *et al*, 1997; Broussard & Damania, 2020). Like many viruses, KSHV manipulates the autophagic machinery, and it does so during both lytic and latent phases. The viral-Bcl-2 (v-Bcl-2) protein binds the autophagy initiator Beclin-1 to interfere with

activation of autophagy during the lytic phase, presumably to limit xenophagic destruction of newly assembled virions (Pattingre *et al*, 2005; Wei *et al*, 2008; Liang *et al*, 2008). The viral FLICE inhibitory protein (v-FLIP), expressed during latency, binds Atg3 to suppress the LC3 lipidation process during autophagosome biogenesis (Lee *et al*, 2009). By contrast, KSHV also expresses a viral cyclin D homolog (v-cyclin), from the same multicistronic latent transcript as v-FLIP; v-cyclin deregulates the cell cycle, causes aberrant host DNA replication, and triggers DNA damage that that leads to autophagy and cellular senescence (Leidal *et al*, 2012). The engagement of autophagy during the transition to cellular senescence is also observed in other systems and is required for the production and non-conventional secretion of pro-inflammatory cytokines such as IL-1β, IL-6 and IL-8 (Young *et al*, 2009), a phenomenon now termed the senescence-associated secretory phenotype (SASP). Clearly, KSHV manipulation of autophagic flux to both prevent xenophagy, fine tune interferon responses, and enhance inflammatory cytokine production during KS is a complicated and highly regulated process about which much remains unknown.

Processing bodies (PBs) are ubiquitous, cytoplasmic, ribonucleoprotein (RNP) granules that regulate expression of many cytokine RNA transcripts, making them important sites of inflammatory control. PBs contain enzymes involved in mRNA turnover including those that mediate decapping (Dcp2 and co-factors Dcp1a and Edc4/Hedls), 5'-3' exonucleolytic degradation (5'-3' exonuclease Xrn1 and RNA helicase Rck/DDX6) and some components of the RNA-induced silencing complex (Cougot *et al*, 2012; Hubstenberger *et al*, 2017; Corbet & Parker, 2019; Youn *et al*, 2018; Riggs *et al*, 2020; Mohamud *et al*, 2019; Luo *et al*, 2018). Approximately one-third of all protein-coding mRNAs are shuttled to PBs for decay and/or repression (Hubstenberger *et al*, 2017). mRNAs are routed to PBs by RNA-binding proteins (RBPs) through recognition of common sequence elements. AU-rich elements (AREs) are one type of RNA regulatory element; they are found in the 3' untranslated regions of ~8% of cellular transcripts and are well-known destabilizing elements that are responsible for targeting RNAs to PBs (Barreau *et al*, 2005; Bakheet *et al*, 2018; García-Mauriño *et al*, 2017). When bound by destabilizing RBPs such as tristetraprolin (TTP) or butyrate response factor-1 (BRF1), ARE-containing RNAs are directed to PBs and suppressed (Maitra *et al*, 2008; Lai *et al*, 1999; Lai & Blackshear, 2001). By contrast, the stabilizing RBP, HuR, shuttles from the nucleus to the cytoplasm where it promotes ARE-mRNA translation (Tran *et al*, 2003; Peng *et al*, 1998). We

111 and others showed that the presence of microscopically visible PBs correlates with the
112 constitutive turnover or translational suppression of ARE-mRNAs; when PBs are lost, this
113 suppression is reversed (Corcoran *et al*, 2012, 2015; Franks & Lykke-Andersen, 2007; Blanco *et*
114 *al*, 2014; Vindry *et al*, 2017). Because ARE-mRNAs code for potent regulatory molecules such
115 as inflammatory cytokines, PBs regulate the production of inflammatory cytokines whose
116 transcripts contain AREs, including IL-6, IL-8, IL-1β, and TNF, and many of these inflammatory
117 molecules are elevated in KS (Ensoli *et al*, 2010; Ensoli & Stürzl, 1998; Lane *et al*, 2002; Miles
118 *et al*, 1990; Riva *et al*, 2010; Sadagopan *et al*, 2007; Salahuddin *et al*, 1988; Bakheet *et al*, 2018).
119 Although PBs are constitutive, they are continuously assembled and disassembled and
120 relatively little is known about how they are regulated (Aizer *et al*, 2014). Stimuli that activate
121 the p38/MK2 MAP kinase pathway as well as many virus infections elicit PB disassembly and a
122 concomitant reduction in ARE-mRNA suppression to promote inflammatory molecule
123 production (Corcoran *et al*, 2012, 2015; Vindry *et al*, 2017; Corcoran & McCormick, 2015;
124 Standart & Weil, 2018; Docena *et al*, 2010). We have previously shown that KSHV causes PB
125 disassembly during latent infection, and that the viral protein Kaposin B (KapB) induces PB
126 disassembly and enhances the production of an ARE-containing reporter (Corcoran *et al*, 2015;
127 Corcoran & McCormick, 2015; Corcoran *et al*, 2011). These data support the notion that PB
128 disassembly is an important contributor to inflammation associated with KS (Corcoran *et al*,
129 2015; Wen & Damania, 2010). Although we know KapB binds and activates the kinase MK2,
130 and that MK2 is an important component of the mechanism of KapB-mediated PB disassembly
131 and ARE-mRNA stabilization, we do not precisely understand how PB loss is elicited by KapB
132 (McCormick & Ganem, 2005; Corcoran *et al*, 2015). The observation that MK2 can
133 phosphorylate Beclin-1 to increase autophagic flux in response to nutrient scarcity (Wei *et al*,
134 2015) suggested to us that KapB may also drive autophagic flux. We now show that the KSHV
135 KapB protein enhances autophagic flux, revealing an additional layer of complexity in viral
136 regulation of autophagy during KSHV latency. We also show that KapB requires canonical
137 autophagy machinery to induce PB disassembly and ARE-mRNA stabilization and that KapB
138 selects PB components for autophagic turnover using the selective autophagy receptor, NDP52,
139 as KapB-mediated PB disassembly and ARE-mRNA reporter expression does not occur when
140 NDP52 is silenced. We had previously observed that a constitutively active form of MK2 elicits
141 PB disassembly and ARE-mRNA stabilization (Corcoran *et al*, 2015); however, we show herein

142 that this mechanism does not rely on canonical or selective autophagy machinery. Our data
143 reveal that cells possess both autophagy-dependent and -independent mechanisms to regulate PB
144 turnover and inflammatory molecule production. These data also forge a new connection
145 between the selective autophagy receptor, NDP52, and cytoplasmic PBs, both of which control
146 innate immune responses and inflammation.
147

148 **Results**

149 **KapB induces autophagic flux**

150 KapB expression activates the stress-responsive kinase MAPKAPK2 (MK2) (McCormick &
151 Ganem, 2005; Corcoran *et al*, 2015). Since MK2 has been shown to phosphorylate the essential
152 autophagy inducer Beclin 1 in response to amino acid starvation (Wei *et al*, 2015; Shen *et al*,
153 2016; Gurkar *et al*, 2013), we wondered if KapB expression promotes autophagic flux. To
154 measure autophagic flux, we performed an LC3 conversion assay (Mizushima *et al*, 2010).
155 Quantification of LC3-II is an indicator of increased autophagosome formation. Because LC3-II
156 itself is a substrate for autophagic degradation, an increase in autophagic flux will not be
157 revealed in conditions without the use of a lysosomal inhibitor treatment, such as Bafilomycin
158 A1 (BafA1) (Mauvezin & Neufeld, 2015). To this end, human umbilical vein endothelial cells
159 (HUVECs) were transduced with lentiviral vectors that express KapB or an empty vector control
160 and treated for increasing times with BafA1; LC3-II accumulation in the presence of BafA1
161 treatment over time was determined by immunoblotting. Over the 4 h BafA1 treatment time
162 course, KapB-expressing cells showed a significant increase in LC3-II compared to vector
163 controls (Fig 1A). We also measured endogenous LC3 puncta using immunofluorescence as an
164 indicator of autophagic flux (Kabeya, 2000; Mizushima *et al*, 2010). Untreated KapB-expressing
165 HUVECs displayed LC3 puncta similar to that of control cells. However, LC3 puncta
166 significantly increased after BafA1 treatment was used to block lysosomal turnover and LC3
167 degradation, further suggesting that KapB expression enhanced autophagic flux (Fig 1B). When
168 KapB-expressing HUVECs were analyzed by electron microscopy, double-membraned vesicles
169 reminiscent of autophagosomes were observed in KapB cells but could not be found in vector
170 control cells (Fig 1C). Taken together, these data show that KapB induces autophagic flux in
171 HUVECs.

172

173 **Canonical autophagy is required for KapB-mediated PB disassembly and ARE-mRNA**
174 **stability**

175 Our group previously described that MK2 activation was an important component of KapB-
176 mediated PB loss (Corcoran *et al*, 2015). However, these experiments did not reveal the precise
177 mechanism of PB loss nor did they clarify if KapB was causing PB disassembly or blocking PB
178 assembly (Corcoran *et al*, 2015). Since PBs are dynamic RNP granules, we decided to determine
179 whether KapB-mediated PB loss was a result of enhanced disassembly of PBs or prevention of
180 their *de novo* assembly. To do so, we utilized HeLa cells that express a Dox-inducible GFP-
181 tagged version of the PB-resident protein, Dcp1a (Youn *et al*, 2018). When fixed, GFP-positive
182 puncta co-stain with endogenous PB proteins such as the RNA helicase DDX6/Rck and the
183 decapping co-factor Hedls/Edc4, indicating that they represent PBs (Fig S1). KapB was
184 transfected into these cells either before or after inducing GFP-Dcp1a granule formation. When
185 KapB was expressed prior to granule induction, Dcp1a puncta formation was intact, although
186 their appearance was slightly delayed compared to vector control cells (Fig S1A). However,
187 when KapB was expressed after granule induction, GFP-positive puncta were lost (Fig S1B).
188 PBs could also be induced by treating cells with sodium arsenite (Fig S1C). Taken together,
189 these results showed that KapB causes PB loss by inducing PB disassembly but that KapB
190 expression does not block PB assembly. These data suggested that KapB may be activating a
191 normal cellular pathway that is important for PB turnover, such as autophagy.

192 To determine whether autophagy was required for KapB-mediated PB disassembly, autophagic
193 flux was inhibited by silencing the canonical autophagy regulator, Atg5. When Atg5 was
194 silenced in KapB-expressing HUVECs, PBs were restored (Fig 2A and B). We then examined
195 PB disassembly in Atg5 -/- MEFs, which are defective for autophagy as indicated by the lack of
196 LC3-II (Fig S2A). KapB failed to disassemble PBs in Atg5 -/- MEFs but did disassemble PBs in
197 matched wild-type controls (Fig 2D and E). Moreover, KapB expression resulted in a significant
198 increase in Atg5 protein levels, consistent with other data that showed KapB is promoting
199 autophagy (Fig 1, 2C). Blocking autophagic degradation with BafA1 also restored PBs in KapB-
200 expressing cells (Fig 3A, B). These data suggest that KapB is accelerating PB turnover by
201 engaging autophagy. We reasoned that if KapB required autophagy for PB turnover, KapB

202 expression should decrease steady-state levels of key PB proteins that have important scaffolding
203 roles for granule formation, such as EDC4/Hedls, Xrn1, DDX6/Rck or Dcp1a (Ayache *et al*,
204 2015). Immunoblotting for these proteins revealed that steady-state levels of the PB-resident
205 protein Dcp1a were reduced in KapB-expressing cells, which was partially restored upon
206 incubation with BafA1 treatment (Fig 3C). However, steady-state levels of other PB-resident
207 proteins were not markedly altered by KapB expression (Fig 3). These data suggest that KapB
208 expression promotes the autophagic degradation of the PB-resident protein Dcp1a, but not all PB
209 proteins. Consistent with these observations, inducing autophagic flux with the mTORC1/2
210 inhibitor Torin (Thoreen *et al*, 2009) decreased the steady-state level of Dcp1a but not other PB
211 proteins, blocking autophagic flux with BafA1 or choroquine increased Dcp1a but blocking
212 proteasomal degradation with MG132 did not influence Dcp1a levels (Fig S3).

213 PBs are nodes of mRNA regulation and microscopically visible PBs are associated with
214 ARE-mRNA degradation (Guo *et al*, 2018; Luo *et al*, 2018; Corcoran *et al*, 2015, 2012; Franks
215 & Lykke-Andersen, 2008; Vindry *et al*, 2017; Blanco *et al*, 2014) After LPS addition to
216 stimulate the transcription of inflammatory RNAs (Nilsen *et al*, 1998), we confirmed enhanced
217 steady state levels for some endogenous ARE-containing RNA transcripts, like IL-6, in KapB-
218 expressing cells (Fig 4A). Because baseline levels of endogenous ARE-mRNAs are normally
219 below a level of accurate detection by RT-qPCR analysis, their analysis requires endothelial cell
220 activation to induce transcription (Nilsen *et al*, 1998), confounding our analysis by the
221 introduction of another variable. For this reason, we utilized a luciferase reporter assay that we
222 previously developed, described in (Corcoran *et al*, 2011) to simplify further studies. Briefly,
223 HeLa cells were co-transfected with a Firefly luciferase (FLuc) construct containing the AU-rich
224 element from CSF2 in its 3'UTR and a Renilla luciferase (RLuc) construct with no ARE;
225 transcription of both reporter constructs was then stopped by the addition of doxycycline. In
226 control (vector transfected) cells, the FLuc-ARE mRNA decayed rapidly and FLuc luminescence
227 relative to the RLuc transfection control was low. KapB expression caused a significant increase
228 in FLuc/RLuc relative luminescence compared to control cells (Fig 4B) as previously shown in
229 (Corcoran *et al*, 2015). This is consistent with our previous work indicating that KapB-mediated
230 PB loss correlated with enhanced luminescence of the ARE-containing luciferase reporter
231 expression because rapid mRNA turnover was reversed and FLuc translation was enhanced
232 (Corcoran *et al*, 2011, 2015). When canonical autophagy was perturbed in KapB-expressing cells

233 by Atg5 silencing, KapB-expressing cells no longer displayed high relative luminescence
234 compared to controls (Fig 4A). Likewise, when KapB-expressing cells were treated with BafA1,
235 relative luminescence was significantly decreased compared to KapB-expressing untreated
236 control cells (Fig 4C). Together, these data showed that canonical autophagy is required for
237 KapB-mediated PB disassembly and the enhanced expression of an ARE-mRNA reporter.
238

239 **Canonical autophagy is not required for MK2-mediated PB disassembly**

240 Because we know that KapB can directly bind and activate MK2 (McCormick & Ganem, 2005)
241 and that MK2 is, in part, required for KapB-mediated effects on PBs and ARE-mRNA (Corcoran
242 *et al*, 2015), we reasoned that a constitutively active version of MK2 would also induce PB
243 disassembly in an autophagy-dependent manner. To test this, we used a construct called MK2EE
244 in which two threonine residues that are normally phosphorylated by p38 MAPK in response to
245 stress signaling are substituted with glutamic acid residues, rendering the kinase constitutively
246 active (Kayyali *et al*, 2002; Rousseau *et al*, 1997). We previously demonstrated that MK2EE
247 causes PB disassembly (Corcoran *et al*, 2015) and others have shown that it can also increase
248 autophagic flux (Wei *et al*, 2015). We confirmed that autophagy was upregulated in MK2EE-
249 expressing HUVECs by staining for endogenous LC3 puncta. We observed that BafA1 treatment
250 resulted in a significant increase in LC3-puncta compared to vector controls, consistent with
251 enhanced autophagic flux (Fig 5A). We then tested if MK2EE-induced PB disassembly was
252 reliant on autophagic flux. MK2EE-expressing HUVECs retained the ability to disassemble PBs
253 after Atg5 silencing (Fig 5B). MK2EE expression was previously shown to increase the
254 FLuc/RLuc relative luminescence in our reporter assay (Corcoran *et al*, 2015) and we reproduced
255 these data herein (Fig 5C). However, Atg5 silencing did not significantly decrease MK2EE-
256 mediated relative luminescence (Fig 5C). These data suggest that although MK2EE induces
257 autophagy and PB disassembly, these are unrelated phenotypes and the manner by which
258 MK2EE induces PB loss does not require canonical autophagy pathways involving Atg5.

259 **KapB-mediated PB disassembly and ARE-mRNA stabilization require the selective**
260 **autophagy receptor NDP52**

261 We wondered if KapB was inducing PB disassembly by promoting the selective autophagy of
262 the entire PB RNP granule or select PB proteins. Very little is known about how PB dynamics

263 are regulated; however, one previous study observed the SAR, NDP52, partially co-localizes
264 with some PB proteins (Guo *et al*, 2014). For this reason, we investigated whether the SARs
265 NDP52, p62, VCP, NBR1 and OPTN were required for KapB-mediated PB disassembly by
266 designing shRNAs to knockdown each of these SARs. Despite trying several different shRNA
267 sequences, our attempts to silence NBR1 were unsuccessful, and shRNAs targeting VCP resulted
268 in significant HUVEC toxicity. Therefore, the role of these molecules in PB turnover could not
269 be determined. Genetic knockdown of NDP52, p62 or OPTN was validated in control and KapB-
270 expressing cells (Fig S2C). In these experiments, silencing of p62 or OPTN did not restore PBs
271 in KapB-expressing cells whereas NDP52 knockdown significantly restored PBs. (Fig 6A and B,
272 Fig S3A). These data pinpointed an important role for NDP52 in the selectivity of KapB-
273 mediated PB disassembly. We also examined whether these SARs were required for KapB-
274 enhanced relative luminescence in our ARE-mRNA reporter assay. Similarly, we found that p62
275 or OPTN knockdown had no effect on KapB-mediated FLuc/RLuc luminescence, but NDP52
276 silencing decreased FLuc/RLuc luminescence compared to non-targeting, KapB-expressing
277 controls (Fig 6C). Therefore, KapB stimulated PB disassembly and concomitant luminescence of
278 our ARE-containing reporter uses a mechanism dependent on the SAR, NDP52.

279 Given that MK2 induces autophagy, but MK2EE-mediated PB disassembly did not require
280 canonical autophagy machinery, we speculated that MK2EE-mediated PB disassembly could be
281 facilitated by NDP52. However, p62, NDP52 and OPTN silencing did not inhibit PB
282 disassembly in MK2EE-expressing cells (Fig S3B, Fig 7A and B). Likewise, silencing of p62,
283 OPTN, or NDP52 did not decrease FLuc/RLuc luminescence in MK2EE-expressing cells as it
284 did in KapB-expressing cells. In fact, NDP52 knockdown increased ARE-mRNA stability (Fig
285 7C), although the significance of this observation is unclear. These data confirm that MK2-
286 mediated PB disassembly and enhanced ARE-containing luciferase reporter expression do not
287 require canonical autophagy or selective autophagy machinery.

288 Previous work has shown that activation of MK2 activation can contribute to a senescence-
289 associated secretory phenotype (SASP) that develops in senescent cells over time and is
290 associated with a pro-inflammatory and pro-tumorigenic environment (Herranz *et al*, 2015). One
291 feature of this activation is the phosphorylation of the ARE-mRNA binding protein, BRF1, by
292 MK2 (Maitra *et al*, 2008). We observed that MK2EE expression induced the phosphorylation of

293 BRF1 while KapB did not (Fig S5). These data suggest that MK2EE induced phosphorylation of
294 BRF1 may be sufficient to prevent ARE-mRNAs from turnover. This distinction could provide a
295 partial explanation for how MK2EE may increase ARE-mRNA reporter activity in an Atg5- and
296 NDP52-independent manner. These data are consistent with a model wherein KapB and MK2 do
297 not use identical mechanisms to mediate PB disassembly and ARE-mRNA stabilization, and that
298 KapB-mediated PB disassembly requires canonical and selective autophagy machinery that is
299 not required for MK2EE-mediated PB loss.

300 **KapB-mediated PB disassembly is rescued by NDP52 but not ubiquitin-binding domain or**
301 **LIR mutants**

302 NDP52 has many functions in selective autophagy and autophagosome maturation and is a
303 crucial adaptor for mitophagy and xenophagy (Ellinghaus *et al*, 2013; Fu *et al*, 2018; Lazarou *et*
304 *al*, 2015; Morriswood *et al*, 2007; Verlhac *et al*, 2015). Structural domains that are important for
305 the function of NDP52 as a SAR include a non-canonical LC3-C interacting region (cLIR) that
306 binds to LC3-decorated autophagosomes and a ubiquitin binding domain (UBD) that binds
307 ubiquitinated cargo proteins, linking them to the autophagosome for engulfment (Figure 8A)
308 To clearly elucidate if NDP52 was required for KapB-mediated PB disassembly because
309 of its ability to promote selective autophagy, we performed a complementation experiment. We
310 first silenced endogenous NDP52 in control or KapB-expressing HUVECs using shRNAs
311 targeting the 3'UTR of NDP52 and verified its knockdown (Fig S2F). Next, NDP52 expression
312 was restored by overexpressing a fluorescently tagged NDP52 construct. Complementation of
313 NDP52-silenced HUVECs with wild-type NDP52 restored KapB-mediated PB disassembly
314 compared to vector controls (Fig 8B and C, S4). We next sought to determine whether the PB
315 disassembly initiated in KapB-expressing cells was reliant on two domains of NDP52 that are
316 important for its role as a SAR: the LIR and UBD. We restored NDP52 expression in NDP52-
317 silenced HUVECs by complementation with a fluorescently tagged UBD mutant (C443K) or a
318 cLIR and UBD combined mutant (V136S and C443K) (Padman *et al*, 2019; Ellinghaus *et al*,
319 2013; Till *et al*, 2013) (Fig 8A). Complementation with either of the mutated forms of NDP52
320 failed to restore KapB-mediated PB disassembly in NDP52-silenced HUVECs. These data
321 indicated that both the UBD and cLIR domains of NDP52 are required for KapB-mediated PB

322 disassembly (Fig 8B and C). These data provide strong evidence to support that the function of
323 NDP52 in selective autophagy is required for its role in KapB-mediated PB disassembly.
324
325

326 **Discussion**

327 In this manuscript we present new data that reveals the KSHV protein, KapB, relies on
328 canonical autophagy machinery and the selective autophagy receptor, NDP52, in order to cause
329 PB disassembly and enhance ARE-containing inflammatory molecule expression. To our
330 knowledge, this is the first report that NDP52 regulates the turnover of endogenous PBs and the
331 first description of the contribution of NDP52 to immune regulation by altering inflammatory
332 cytokine RNA turnover/suppression in PBs. Our major findings are as follows: i) KapB
333 increased autophagic flux, thereby contributing to the complex regulation of autophagic
334 processes during KSHV latent infection and tumourigenesis, ii) KapB-mediated PB disassembly
335 and enhanced translation of an ARE-containing reporter required canonical autophagy machinery
336 and the selective autophagy receptor, NDP52, iii) KapB-mediated PB disassembly proceeds by a
337 mechanism that is autophagy-dependent and differs from that induced by the constitutively
338 active kinase, MK2 (MK2EE), which induces PB disassembly independent of canonical (Atg5)
339 and selective autophagy (NDP52) machinery. Taken together these results reveal that cellular PB
340 turnover is mediated by autophagy-dependent and -independent mechanisms and that a viral
341 protein co-opts NDP52 selective autophagy to amplify PB turnover. In so doing, KapB enhances
342 the translation of ARE-containing RNAs, transcripts that encode potent inflammatory molecules
343 that would normally be subject to constitutive decay or suppression in PBs. This mechanism is
344 another example of the ingenuity with which viruses co-opt cellular processes and reveals a
345 novel regulatory network that links the NDP52 to inflammatory molecule production via PB
346 catabolism.

347 MK2 activation promotes autophagy by phosphorylating Beclin 1 (Wei *et al*, 2015);
348 therefore, we hypothesized that the MK2-activating viral protein KapB (McCormick & Ganem,
349 2005) utilized autophagy to promote PB clearance. However, our data showed that although both
350 KapB and MK2EE increased autophagic flux (Fig 1, Fig 5), only KapB-mediated PB
351 disassembly required Atg5 and the selective autophagy functions of the SAR, NDP52 (Fig 6, Fig
352 7). MK2EE does not use an autophagy-dependent mechanism, as KapB does, for PB
353 disassembly, and our studies have not yet revealed a connection between PB loss and
354 degradative machinery in these cells. These data imply that cells utilize more than one pathway
355 to disassemble PBs, consistent with the dual mechanism responsible for turnover of other RNP

356 granules like stress granules (Buchan *et al*, 2013; Turakhiya *et al*, 2018). Our data is also
357 supported by previous work showing that in yeast, PB recycling requires canonical autophagy
358 machinery and in mammalian cells NDP52 colocalizes with a GFP-tagged version of Dcp1a
359 when overexpressed (Buchan *et al*, 2013; Guo *et al*, 2014). We add significantly to these studies,
360 by performing our work in primary human endothelial cells and by staining for endogenous PBs
361 using immunofluorescence for the decapping co-factor EDC4/Hedls. We reveal that when KapB
362 is expressed, endogenous PBs are lost via Atg5- and NDP52-dependent autophagic flux. We also
363 complemented NDP52-silenced cells with shRNA-resistant NDP52 and observed the restoration
364 of KapB-mediated PB disassembly when complementation was performed with wild-type
365 constructs but not those lacking the LIR or UBD regions (Fig 8). These data indicate that it is the
366 ability of NDP52 to act as a SAR that is required for KapB-mediated PB turnover, and that this
367 mechanism may involve NDP52 binding to a ubiquitinated PB protein(s). This coincides with
368 observations that ubiquitination promoted cargo binding and identification by SARs, including
369 NDP52 (Shaid *et al*, 2013) while the removal of the UBD rendered NDP52 unable to localize to
370 and bind cargo, such as *Salmonella typhimurium* (Cemma *et al*, 2011; Xie *et al*, 2015).
371 Immunoelectron microscopy showed that PBs range in size from 150 to 350 nm and
372 possess an external area of peripheral protrusions that contain the helicase Rck/DDX6 (Cougot *et*
373 *al*, 2012). These protrusions are anchored to a dense central core of decay enzymes, including
374 Dcp1a and Xrn1. Disruption of the PB outer ring by silencing DDX6 revealed that the peripheral
375 structure and/or DDX6 itself is required for PB stability (Cougot *et al*, 2012). Other PB-localized
376 enzymes are also required for PB stability, including Dcp1a; however, only three PB proteins are
377 required for *de novo* PB formation, DDX6, the translation suppressor, 4E-T, and LSM14a
378 (Ayache *et al*, 2015). Our data showed that KapB expression decreased the steady-state levels of
379 Dcp1a and BafA1 treatment partially restored Dcp1a, while KapB expression had little effect on
380 the steady-state levels of other PB proteins (Fig 3). Inducing autophagy with the mTORC1/2
381 inhibitor Torin recapitulated this effect, decreasing steady-state levels of Dcp1a, but not other PB
382 proteins like Xrn1, EDC4/Hedls or DDX6 (Fig S3). Blocking the degradative step of autophagy
383 using BafA1 or chloroquine increased steady-state Dcp1a but blocking the proteasome with
384 MG132 did not (Fig S3). These data support our model that the entire PB granule is not
385 autophagocytosed, but PB disassembly is induced by the selective autophagic targeting of one or
386 more PB proteins, likely including Dcp1a, and that when a critical amount of Dcp1a/other PB

387 protein is degraded, the PB disassembles. Consistent with this, we show that PBs can still form
388 even during KapB expression, if we overexpress Dcp1a-GFP or block translation using sodium
389 arsenite (Fig S1). Taken together, this means the most likely PB protein candidate for autophagic
390 degradation in our model is Dcp1a, as its steady-state levels are significantly reduced by both
391 KapB expression and Torin and Dcp1a is important for PB stability (Ayache *et al*, 2015). Dcp1a
392 is also targeted by other viruses that mediate PB disassembly; for example, infection with
393 poliovirus also caused PB disassembly and the loss of Dcp1a over a time course of infection
394 (Dougherty *et al*, 2011).
395 We do not yet understand how KapB expression may alter Dcp1a to promote its targeting
396 to the autophagosome, but we predict that KapB expression may change Dcp1a function and
397 localization via one or more post-translational modifications. Relatively little is known about the
398 regulation of PB form and function by the post-translational modification of PB components.
399 Many PB proteins, including Dcp1a, EDC4/Hedls, Dcp2 and DDX6, are phosphorylated;
400 however, the functional consequences of these phosphorylation events for PB granule formation
401 is not fully appreciated (Bish *et al*, 2015; Gustafson & Wessel, 2010; Rahman *et al*, 2014; Yoon
402 *et al*, 2010). In the case of Dcp1a, its mono-phosphorylation at serine 315 stabilized its
403 interaction with the catalytic component of the decapping complex, Dcp2; however, its
404 hyperphosphorylation coincided with PB loss, showing that Dcp1a phosphorylation status
405 regulates PB dynamics (Tenekeci *et al*, 2016; Aizer *et al*, 2013; Chiang *et al*, 2013). PB proteins
406 including Dcp1a, Dcp2 and EDC3 are also ubiquitinated, and manipulation of total cellular K63-
407 ubiquitination altered PB formation and function and changed the mRNA half-life of selected
408 cytokine transcripts in a gene-specific manner (Tenekeci *et al*, 2016). These authors also showed
409 that Dcp1a ubiquitination primes the molecule for subsequent phosphorylation, revealing a
410 complex regulatory relationship between these two modifications (Tenekeci *et al*, 2016). We
411 hypothesize that KapB expression promotes the K63-ubiquitination and/or phosphorylation of
412 Dcp1a and that this modification permits its recognition by NDP52. In our model, NDP52
413 binding is a key step in the delivery of Dcp1a (or another unidentified PB protein) to the nascent
414 autophagosome for selective degradation (Fig 9). Experiments are ongoing to test this intriguing
415 model. NDP52 is required for the baseline selective autophagic turnover of innate immune
416 molecules, an effect which can be increased by signals that activate stress-responsive kinases
417 (TNF or IL-1, as examples) or virus infection, and as we show here, a viral protein (Wu *et al*,

418 2020). Therefore, NDP52-mediated selective autophagy is emerging as a central feature of our
419 antiviral response to infection that may be intentionally targeted by viruses.
420
421 The role of autophagy in cellular homeostasis extends beyond its contribution to the
422 recycling of cellular components required for cell survival, as autophagy is now appreciated to
423 balance and modulate immune activation and inflammation (Deretic & Levine, 2018).
424 Autophagy was first reported to dampen inflammation, via an observed association between
425 chronic inflammatory diseases such as Crohn's disease and ulcerative colitis and genetic
426 polymorphisms in genes that regulate diverse steps of autophagy, including NDP52 (Ellinghaus
427 *et al*, 2013; Henckaerts *et al*, 2011; Hampe *et al*, 2007). One of the best characterized ways that
428 autophagy dampens inflammatory signals is via p62-mediated selective autophagy of
429 inflammasome complexes that, when active, process precursor cytokines like IL-1β into its
430 mature secreted form (Lamkanfi & Dixit, 2014; Shi *et al*, 2012). However, autophagy does not
431 always negatively regulate inflammation, and autophagic machinery has also been shown to
432 facilitate the unconventional secretion of IL-1β (Zhang *et al*, 2015; Dupont *et al*, 2011) or
433 promote cytokine responses to virus infection (Law *et al*, 2010). More recently, selective
434 autophagy receptors have been shown to target several innate immune factors for degradation
435 (Chen *et al*, 2016; Du *et al*, 2018; Jin *et al*, 2017; Prabakaran *et al*, 2018; Yang *et al*, 2017; He *et*
436 *al*, 2019). In particular, in response to viral infection, NDP52 has been shown to control the
437 autophagic turnover of the transcription factor IRF3, an indispensable player in the interferon
438 response, and mediate the turnover of the signaling molecule, MAVS (Wu *et al*, 2020; Jin *et al*,
439 2017). Clearly the influence of cell autonomous autophagy machinery on innate immune
440 responses and inflammatory cytokine production is a complex process about which much
441 remains undiscovered (summarized in Ahmad et al., 2018).

442 Infection with KSHV induces high levels of pro-inflammatory cytokines, chemokines
443 and angiogenic factors such as TNF, IL-1α, IL-1β, IL-6, CXCL8, IFN-γ, VEGF, COX-2 and
444 GM-CSF (Ensoli *et al*, 2010; Ensoli & Stürzl, 1998; Lane *et al*, 2002; Miles *et al*, 1990; Riva *et*
445 *al*, 2010; Sadagopan *et al*, 2007; Salahuddin *et al*, 1988). Although several KSHV proteins
446 promote the transcription of these inflammatory products, many harbor AREs in the 3'UTR of
447 their cognate mRNA, meaning their transcripts are subject to additional post-transcriptional
448 regulation in PBs. We previously showed that KapB and the lytic KSHV protein, viral G-protein-

449 coupled receptor (vGPCR) enhanced the translation of an ARE-containing reporter and elevated
450 steady-state levels of inflammatory products, and that this coincided with the ability of KapB and
451 vGPCR to induce PB disassembly (Corcoran *et al*, 2015, 2012, 2011; McCormick & Ganem,
452 2005). We now show that KapB expression increased the steady-state levels of three ARE-
453 containing transcripts, IL-6, GM-CSF, and TNF (Fig 4A), consistent with previous studies
454 (King, 2013) and coincident with PB disassembly. However, KapB expression did not increase
455 CXCL8 (Fig 4A), indicating that there remains additional regulation, beyond PB disassembly, of
456 ARE-mRNA decay (Palanisamy *et al*, 2008, 2012). This is consistent with other studies showing
457 gene-specific regulation of inflammatory transcripts, even among those grouped together,
458 because the presence of an ARE subjects them to rapid turnover (Tenekeci *et al*, 2016). We also
459 show that the ability of KapB to induce PB disassembly and enhance our ARE-mRNA reporter
460 requires both canonical and selective autophagic machinery (Figs 2-4, 6, 8) while MK2EE-
461 induced PB disassembly and ARE-mRNA reporter expression does not (Fig 5, 7). Our model
462 supports an important role for Dcp1a in the constitutive translational suppression of our ARE-
463 mRNA reporter, and when levels of Dcp1a decrease after KapB expression, more reporter is
464 translated. This is supported by data from other groups that show Dcp1a associates directly with
465 ARE-mRNAs, recruited there by destabilizing RBPs such as TTP and BRF-1 (Chiang *et al*,
466 2013; Lykke-Andersen & Wagner, 2005). We observed that MK2EE expression, but not KapB,
467 resulted in phosphorylation of BRF-1 (Fig S5). BRF-1 is an RBP that binds ARE-containing
468 RNAs and targets them for decay or suppression; this decay-promoting activity is dampened by
469 MK2-mediated phosphorylation of BRF-1 at four sites (Maitra *et al*, 2008). It is possible that the
470 phosphorylation of BRF-1 in MK2EE-expressing cells is sufficient to prevent ARE-mRNA
471 recruitment to Dcp1a and other PB decay factors, but that in KapB-expressing cells,
472 unphosphorylated BRF-1 remains able to bind ARE-RNAs and recruit them to PBs, necessitating
473 autophagic PB turnover as a mechanism to reverse ARE-mRNA reporter repression. These data
474 provide a partial explanation for how MK2EE may enhance the translation of our ARE-
475 containing luciferase reporter independent of autophagy, but do not yet reveal the nature of PB
476 disassembly in these cells.
477 RNA transcripts for some canonical autophagy proteins in the Atg5-Atg12-Atg16
478 complex are also regulated post-transcriptionally by 3'UTR AREs, suggesting that expression of
479 KapB, MK2EE or vGPCR may cause a pro-autophagic positive feedback loop via PB

480 disassembly, enhancing translation of pro-autophagic products. (Lystad *et al*, 2019; Ji *et al*,
481 2019). This is consistent with our observation that KapB-expressing cells displayed increased
482 steady-state levels of Atg5 (Fig 2). Enhanced translation of these mRNAs may also be aided by
483 KapB-mediated upregulation of the stabilizing RBP, HuR (Yoo *et al*, 2010). This feed-forward
484 loop likely contributes to KapB and MK2EE induction of autophagic flux; however, no
485 published report shows that vGPCR increases autophagic flux. In fact, autophagic degradation
486 controls vGPCR protein levels and dampens its pro-tumourigenic, proinflammatory signaling
487 (Wei *et al*, 2015; Dong *et al*, 2016). Taken together, our study reveals a novel way that KSHV
488 infection manipulates autophagic machinery in a cell intrinsic manner to induce PB turnover and
489 promote inflammatory molecule production. The fact that KSHV encodes more than one protein
490 that reverses the constitutive repression of inflammatory mRNAs in PBs highlights its central
491 importance.

492 Autophagy plays a dual role in cancer development mediated by oncogenic viruses
493 (Vescovo *et al*, 2020). Autophagy is initially tumour suppressive, promoting degradation of
494 damaged organelles, preserving genomic stability, and removing pathogens. In cancers of viral
495 origin, like KS, viral inhibition of autophagic flux can help control xenophagy of new viral
496 particles and aid in the establishment of latent infection (Jang *et al*, 2016). However, once cancer
497 is established, autophagic flux promotes progression of established tumours by a variety of
498 approaches, including promoting a pro-tumourigenic and proinflammatory environment
499 (Vescovo *et al*, 2020; Liu & Debnath, 2016). Consistent with this, markers of upregulated
500 autophagic flux are elevated in several cancers and in primary effusion lymphoma cells that
501 harbour the KSHV genome as a latent episome (Pringle et al., 2019; reviewed in Wu et al.,
502 2012), suggesting that at this latent stage, viral gene products enhance autophagy to maintain
503 tumourigenesis. This sensible model is, in reality, an oversimplification, as we know that KSHV
504 gene products both enhance and block autophagic flux during both latent and lytic KSHV phases
505 (Vescovo *et al*, 2020; Cirone, 2018). In latency, two viral proteins have previously defined roles
506 in autophagy, vCyclin and vFLIP (Leidal *et al*, 2012; Lee *et al*, 2009). vCyclin has been shown
507 to induce oncogene-induced senescence through induction of autophagy, whereas vFLIP works
508 to counteract vCyclin by blocking autophagy through binding Atg3 and inhibiting LC3 lipidation
509 (Leidal *et al*, 2012; Lee *et al*, 2009). We show here that KapB also upregulates autophagic flux,
510 opposing the activity of vFLIP during viral latency. We do not yet know the precise impact of

511 latent gene co-expression on autophagy regulation; however, the observation that latently
512 infected B-lymphocytes displayed elevated autophagic flux suggest that a pro-autophagic
513 phenotype dominates during KSHV latency (Pringle *et al*, 2019). We predict that KapB, in
514 concert with vCyclin, promotes autophagy and that vFLIP expression works to fine tune this
515 mechanism.

516 One possible way that KSHV latent genes cooperate to fine tune autophagy during
517 KSHV latency may involve viral dysregulation of the cellular transcription factor, Nrf2. Nrf2 is
518 responsible for the activation of several antioxidant response genes but also induces expression
519 of NDP52 to promote selective autophagy (Jo *et al*, 2014; Moi *et al*, 1994; Nguyen *et al*, 2009).
520 Nrf2 activity is upregulated by KSHV *de novo* infection of endothelial cells and during KSHV
521 latency, as evidenced by the nuclear translocation of Nrf2, which is normally retained in the
522 cytoplasm by its negative regulator, Keap1, and the expression of Nrf2 target genes (Gjyshi *et al*,
523 2014). The mechanism for KSHV Nfr2 activation was revealed to utilize vFLIP, which blocks
524 autophagy and leads to an accumulation of the SAR, p62, that in turn promotes the degradation
525 of Keap1 and the stabilization of Nrf2 (Gjyshi *et al*, 2015). In this manner, vFLIP may indirectly
526 promote the selective autophagy of PBs during KSHV latency by increasing NDP52 expression.
527 This activity may synergize with the activities of KapB we propose in our model, wherein we
528 predict that KapB expression induces an unknown post translational modification of the PB
529 protein, Dcp1a, promoting its selection as autophagic cargo by NDP52 (Fig 9).

530 Taken together, our data and that of others support that viral KSHV enhancement of
531 autophagy is central to latent viral tumourigenesis and the creation of a proinflammatory
532 environment and may also play an important role in regulating the balance between latent versus
533 lytic gene expression for KSHV and related herpesviruses (Dong *et al*, 2016; Park *et al*, 2016;
534 Wang *et al*, 2019). Although this may suggest that targeting autophagic processes could be a
535 useful strategy for treating KS, as supported by the regression of iatrogenic KS lesions after
536 treatment with the mTORC1 complex inhibitor and autophagy inducer, rapamycin (Stallone *et*
537 *al*, 2005), the complicated balance of autophagy regulation by KSHV suggests the need for more
538 selective therapies. Our study of the KSHV protein, KapB, has unveiled such an opportunity,
539 revealing the potential utility of targeting NDP52-dependent selective catabolism of PBs to limit
540 pathological and pro-tumourigenic inflammation.

541

542 **Materials and Methods**

543 **Cell culture**

544 All cells were grown at 37 °C with 5% CO_2 and 20% O_2. HEK293T cells (ATCC), HeLa Tet-Off
545 cells (Clontech), Atg5 +/+ and -/- MEFs (Kuma *et al*, 2004), and HeLa Flp-In TREx GFP-Dcp1a
546 cells (a generous gift from Anne-Claude Gingras) were cultured in DMEM (Thermo Fisher)
547 supplemented with 100 U/mL penicillin, 100 µg/mL streptomycin, 2 mM L-glutamine (Thermo
548 Fisher) and 10% FBS (Thermo Fisher). HUVECs (Lonza) were cultured in endothelial cell
549 growth medium (EGM-2) (Lonza). HUVECs were seeded onto gelatin (1% w/v in PBS)-coated
550 tissue culture plates or glass coverslips. All drug treatments were performed for the times
551 indicated in each experiment at the concentrations listed in Table 6.

552 **Cloning**

553 All shRNAs were generated by cloning shRNA hairpin sequences found in Table 2 into pLKO.1-
554 TRC Puro (pLKO.1-TRC cloning vector was a gift from David Root (Addgene plasmid # 10878;
555 http://n2t.net/addgene:10878; RRID:Addgene_10878) or pLKO.1-blast (pLKO.1-blast was a gift
556 from Keith Mostov (Addgene plasmid #26655; http://n2t.net/addgene:26655;
557 RRID:Addgene_26655). pBMN mCherry-NDP52(C443K) was a gift from Michael Lazarou
558 (Addgene plasmid #119685; http://n2t.net/addgene:119685; RRID:Addgene_119685) and
559 pBMN mCherry-NDP52(V136S/C443K) was a gift from Michael Lazarou (Addgene plasmid
560 #119686; http://n2t.net/addgene:119686; RRID:Addgene_119686). The overexpression
561 plasmids, pLJM1 mCh-NDP52 C443K and pLJM1 mCh-NDP52 C443K V136S were made
562 using the primers in Table 4 to clone NDP52 into pLJM1 (Johnston *et al*, 2019).

563 **Lentivirus Production and Transduction**

564 All lentiviruses were generated using a second-generation system. Briefly, HEK293T cells were
565 transfected with pSPAX2, MD2G, and the plasmid containing a gene of interest or hairpin using
566 polyethylimine (PEI, Polysciences). psPAX2 was a gift from Didier Trono (Addgene plasmid
567 #12260; http://n2t.net/addgene:12260; RRID:Addgene_12260) and pMD2.G was a gift from
568 Didier Trono (Addgene plasmid #12259; http://n2t.net/addgene:12259; RRID:Addgene_12259).

569

570 Viral supernatants were harvested 48 h post-transfection, clarified using a 0.45 µ
571 polyethersulfone filter (VWR), and frozen at -80°C until use. For transduction, lentiviruses were
572 thawed at 37°C and added to target cells in complete media containing 5 µg/mL polybrene
573 (Sigma) for 24 h. The media was changed to selection media containing 1 µg/mL puromycin or 5
574 µg/mL blasticidin (Thermo) and cells were selected for 48 h before proceeding with
575 experiments.

576 **Immunofluorescence**

577 Cells were seeded onto coverslips for immunofluorescence experiments and fixed for 10 mins at
578 37 °C in 4% (v/v) paraformaldehyde (Electron Microscopy Sciences). Samples were
579 permeabilized with 0.1% (v/v) Triton X-100 (Sigma-Aldrich) for 10 min at room temperature
580 and blocked in 1% human AB serum (Sigma-Aldrich) for 1 h at room temperature. For
581 autophagosome immunofluorescence cells were fixed for 10 min in ice cold methanol at -20 °C
582 and blocked in 1% human AB serum for 1 h at room temperature. Primary and secondary
583 antibodies were diluted in 1% human AB serum and used at the concentrations in Table 1.
584 Samples were mounted with Prolong Gold AntiFade mounting media (Thermo). For CellProfiler
585 quantification of puncta, samples were incubated with WGA AlexaFluor-647 at a 1:400 dilution
586 for 10 min prior to permeabilization. Image analysis was performed using CellProfiler
587 (cellprofiler.org), an open source platform for image analysis (Carpenter et al., 2006);
588 quantification of puncta was performed as previously described (Castle *et al*, 2020).

589 **Immunoblotting**

590 Cells were lysed in 2x Laemmli buffer and stored at -20°C until use. The DC Protein Assay
591 (Bio-Rad) was used to quantify protein concentration as per the manufacturer's instructions. 10-
592 15 µg of protein lysate was resolved by SDS-PAGE on TGX Stain-Free acrylamide gels
593 (BioRad). Total protein images were acquired from the PVDF membranes after transfer on the
594 ChemiDoc Touch Imaging system (BioRad). Membranes were blocked in 5% bovine serum
595 albumin (BSA) or skim milk in Tris-buffered saline-Tween20 (TBS-T). Primary and secondary
596 antibodies were diluted in 2.5% BSA or skim milk, dilutions can be found in Table 1.

597 Membranes were visualized using Clarity Western ECL substrate and the ChemiDoc Touch
598 Imaging system (BioRad).

599 **Luciferase Assays**

600 Luciferase assays were performed as previously described (Corcoran *et al*, 2011). HeLa Tet-Off
601 cells were transduced with recombinant lentivirus expressing different shRNAs and selected.
602 Cells were transfected according to Corcoran *et al.* (2011) with pTRE2 Firefly Luciferase ARE,
603 pTRE2 Renilla Luciferase, and the expression plasmid of interest using Fugene HD (Promega).
604 Luciferase and renilla activity were quantified using the Dual Luciferase Assay Kit (Promega)
605 and read on a GloMax multi-detection system (Promega).

606 **Quantitative PCR**

607 RNA was collected using a RNeasy Plus Mini Kit (Qiagen) according to the manufacturer's
608 instructions and stored at -80°C until further use. RNA concentration was determined and was
609 reverse transcribed using Maxima H Minus First Strand cDNA Synthesis Kit (Thermo Fisher)
610 using a combination of random and oligo (dT) primers according to the manufacturer's
611 instructions. cDNA was diluted 1:5 for all qPCR experiments and GoTaq qPCR Master Mix
612 (Promega) was used to amplify cDNA. The ΔΔquantitation cycle (Cq) method was used to
613 determine the fold change in expression of target transcripts. qPCR primer sequences can be
614 found in Table 3.

615 **Electron Microscopy**

616 HUVECs were transduced with vector or KapB and selected with 5 µg/mL blasticidin. Cells
617 were washed with PBS and fixed in the plate with 2.5% glutaraldehyde at 4°C overnight. After
618 fixation, cells were scraped in the fixative and pelleted at 300 x *g* for 5 minutes. Samples were
619 sent to the Dalhousie University Electron Microscopy Core Facility for processing and
620 sectioning. Briefly, samples were washed with 0.1% sodium cacodylate buffer, fixed in 1%
621 osmium tetroxide, and stored in 0.25% uranyl acetate at 4ºC. Samples were dehydrated in a
622 graduated series of acetone, infiltrated with epon araldite resin, and embedded in 100% epon
623 araldite resin in a 60ºC oven for 48 h. Sections were cut with a Reichart-Jung Ultracut E
624 Ultramicrotome at approximately 100 nm thick and placed on a 300 mesh copper grid. Samples
625 were stained with 2% aqueous uranyl acetate and lead citrate before being dried and imaged on a

626 JEOL JEM 1230 Electron Microsope at 80kV; pictures were obtained with a Hamamatsu
627 ORCA-HR digital camera.

628 **Statistics**

629 Data shown are the mean ± standard error of the mean (SEM). Statistical significance was
630 determined using a one-way ANOVA, a 2-way ANOVA or Student's t-test when appropriate
631 with the applicable post-test (indicated in the corresponding figure legends). For ANOVAs,
632 matched data from each replicate was paired for analysis. All statistics were performed using
633 GraphPad Prism v.9.0.

634

635 **Acknowledgements**

636 The authors would like to dedicate this manuscript to Dr. Beth Levine, who was a leader in the
637 field of autophagy and viruses and who inspired this work. We sincerely thank the members of
638 the Corcoran lab for helpful discussions about this work, especially Ms. Mariel Kleer. We would
639 like to thank Dr. Craig McCormick (Dalhousie University) for valuable feedback on this
640 manuscript and the McCormick lab for plasmids, expertise and advice. We would like to thank
641 Mr. Stephen Whitefield and Ms. Mary Ann Trevors in the Dalhousie *CORES* (Cellular and
642 Molecular Digital Imaging and Electron Microscopy core facilities) and Dr. Anne Vaahtokari of
643 the Charbonneau Microscopy Facility, UCalgary for microscopy support. We would like to thank
644 Dr. Andreas Till (University of Bonn), Dr. Anne-Claude Gingras (Lunenfeld-Tanenbaum
645 Research Institute) and Dr. Don Ganem (Novartis) for sharing valuable reagents. Model figure
646 created with BioRender. GKS was supported by a CIHR CGS-M scholarship and Scotia Scholars
647 NSHRF graduate training award. ELC was supported by a Killam predoctoral scholarship, an
648 NSERC CGS-M scholarship, and a Nova Scotia Graduate scholarship. Operating funds to
649 support this work derive from a CIHR Project Grant PJT-153210 to JAC.

650

651 **Author Contributions**

652 Carolyn-Ann Robinson: Conceptualization, Experimentation, Analysis, Paper Writing

653 Gillian K. Singh: Conceptualization, Experimentation, Analysis, Paper Writing

654 Elizabeth L. Castle: Analysis

655 Bre Q. Boudreau: Experimentation

656 Jennifer A. Corcoran: Conceptualization, Experimentation, Supervision, Funding Acquisition,
657 Project Administration, Paper Writing

658

659 **Conflict of Interest**

660 The authors have no competing interests to declare.

661

662 **References**

663 Ahmad L, Mostowy S & Sancho-Shimizu V (2018) Autophagy-virus interplay: From cell
664 biology to human disease. *Front Cell Dev Biol* 6

665 Aizer A, Kafri P, Kalo A & Shav-Tal Y (2013) The P Body Protein Dcp1a Is Hyper-
666 phosphorylated during Mitosis. *PLoS One* 8: e49783

667 Aizer A, Kalo A, Kafri P, Shraga A, Ben-Yishay R, Jacob A, Kinor N & Shav-Tal Y (2014)
668 Quantifying mRNA targeting to P-bodies in living human cells reveals their dual role in
669 mRNA decay and storage. *J Cell Sci* 127: 4443–56

670 Ayache J, Bénard M, Ernoult-Lange M, Minshall N, Standart N, Kress M & Weil D (2015) P-
671 body assembly requires DDX6 repression complexes rather than decay or Ataxin2/2L
672 complexes. *Mol Biol Cell* 26: 2579–2595

673 Bakheet T, Hitti E & Khabar KSA (2018) ARED-Plus: An updated and expanded database of
674 AU-rich element-containing mRNAs and pre-mRNAs. *Nucleic Acids Res* 46: D218–D220

675 Balgi AD, Fonseca BD, Donohue E, Tsang TCF, Lajoie P, Proud CG, Nabi IR & Roberge M
676 (2009) Screen for chemical modulators of autophagy reveals novel therapeutic inhibitors of
677 mTORC1 signaling. *PLoS One* 4

678 Barreau C, Paillard L & Osborne HB (2005) AU-rich elements and associated factors: Are there
679 unifying principles? *Nucleic Acids Res* 33: 7138–7150

680 Birgisdottir ÅB, Lamark T & Johansen T (2013) The LIR motif - crucial for selective autophagy.
681 *J Cell Sci* 126: 3237–47

682 Bish R, Cuevas-Polo N, Cheng Z, Hambardzumyan D, Munschauer M, Landthaler M & Vogel C
683 (2015) Comprehensive Protein Interactome Analysis of a Key RNA Helicase: Detection of
684 Novel Stress Granule Proteins. *Biomolecules* 5: 1441–66

685 Blanco FF, Sanduja S, Deane NG, Blackshear PJ & Dixon D a (2014) Transforming growth
686 factor β regulates P-body formation through induction of the mRNA decay factor
687 tristetraprolin. *Mol Cell Biol* 34: 180–95

688 Broussard G & Damania B (2020) Regulation of KSHV Latency and Lytic Reactivation. *Viruses*
689 12

690 Buchan JR, Kolaitis R, Taylor JP & Parker R (2013) Eukaryotic Stress Granules Are Cleared by
691 Autophagy and Cdc48 / VCP Function. *Cell* 153: 1461–1474

692 Castle EL, Douglas P, Rinker KD & Corcoran JA (2020) Viral manipulation of a novel
693 mechanoresponsive signaling axis disassembles processing bodies. *bioRxiv*:
694 2020.05.15.091876 [PREPRINT]

695 Cemma M, Kim PK & Brumell JH (2011) The ubiquitin-binding adaptor proteins p62/SQSTM1
696 and NDP52 are recruited independently to bacteria-associated microdomains to target
697 Salmonella to the autophagy pathway. *Autophagy* 7: 341–5

698 Cesarman E, Chang Y, Moore PS, Said JW & Knowles DM (1995) Kaposi's sarcoma-associated
699 herpesvirus-like DNA sequences in AIDS-related body-cavity-based lymphomas. *N Engl J*
700 *Med* 332: 1186–1191

701 Chang Y, Cesarman E, Pessin MS, Lee F, Culpepper J, Knowles DM & Moore PS (1994)
702 Identification of herpesvirus-like DNA sequences in AIDS-associated Kaposi's sarcoma.
703 *Science* 266: 1865–9

704 Chen M, Meng Q, Qin Y, Liang P, Tan P, He L, Zhou Y, Chen Y, Huang J, Wang RF, *et al*
705 (2016) TRIM14 Inhibits cGAS Degradation Mediated by Selective Autophagy Receptor
706 p62 to Promote Innate Immune Responses. *Mol Cell* 64: 105–119

707 Chiang PY, Shen YF, Su YL, Kao CH, Lin NY, Hsu PH, Tsai MD, Wang SC, Chang GD, Lee
708 SC, *et al* (2013) Phosphorylation of mRNA Decapping Protein Dcp1a by the ERK
709 Signaling Pathway during Early Differentiation of 3T3-L1 Preadipocytes. *PLoS One* 8

710 Cirone M (2018) EBV and KSHV infection dysregulates autophagy to optimize viral replication,
711 prevent immune recognition and promote tumorigenesis. *Viruses* 10

712 Corbet GA & Parker R (2019) RNP granule formation: Lessons from P-bodies and stress
713 granules. *Cold Spring Harb Symp Quant Biol* 84: 203–215

714 Corcoran JA, Johnston BP & McCormick C (2015) Viral activation of MK2-hsp27-
715 p115RhoGEF-RhoA signaling axis causes cytoskeletal rearrangements, p-body disruption
716 and ARE-mRNA stabilization. *PLoS Pathog* 11: e1004597

717 Corcoran JA, Khaperskyy DA, Johnston BP, King CA, Cyr DP, Olsthoorn A V. & McCormick
718 C (2012) Kaposi's Sarcoma-Associated Herpesvirus G-Protein-Coupled Receptor Prevents
719 AU-Rich-Element-Mediated mRNA Decay. *J Virol* 86: 8859–8871

720 Corcoran JA, Khaperskyy DA & McCormick C (2011) Assays for monitoring viral manipulation
721 of host ARE-mRNA turnover. *Methods* 55: 172–181

722 Corcoran JA & McCormick C (2015) Viral activation of stress-regulated Rho-GTPase signaling
723 pathway disrupts sites of mRNA degradation to influence cellular gene expression. *Small*
724 *GTPases* 6: 178–185

725 Cougot N, Cavalier A, Thomas D & Gillet R (2012) The Dual Organization of P-bodies
726 Revealed by Immunoelectron Microscopy and Electron Tomography. *J Mol Biol* 420: 17–
727 28

728 Decker LL, Shankar P, Khan G, Freeman RB, Dezube BJ, Lieberman J & Thorley-Lawson DA
729 (1996) The Kaposi sarcoma-associated herpesvirus (KSHV) is present as an intact latent
730 genome in KS tissue but replicates in the peripheral blood mononuclear cells of KS patients.
731 *J Exp Med* 184: 283–8

732 Deretic V & Levine B (2018) Autophagy balances inflammation in innate immunity. *Autophagy*
733 14: 243–251

734 Docena G, Rovedatti L, Kruidenier L, Fanning Á, Leakey NAB, Knowles CH, Lee K, Shanahan
735 F, Nally K, McLean PG, *et al* (2010) Down-regulation of p38 mitogen-activated protein
736 kinase activation and proinflammatory cytokine production by mitogen-activated protein
737 kinase inhibitors in inflammatory bowel disease. *Clin Exp Immunol* 162: 108–115

738 Dong X, Cheng A, Zou Z, Yang YS, Sumpter RM, Huang CL, Bhagat G, Virgin HW, Lira SA &
739 Levine B (2016) Endolysosomal trafficking of viral G protein-coupled receptor functions in
740 innate immunity and control of viral oncogenesis. *Proc Natl Acad Sci U S A* 113: 2994–
741 2999

742 Dougherty JD, White JP & Lloyd RE (2011) Poliovirus-mediated disruption of cytoplasmic
743 processing bodies. *J Virol* 85: 64–75

744 Du Y, Duan T, Feng Y, Liu Q, Lin M, Cui J & Wang R (2018) LRRC25 inhibits type I IFN
745 signaling by targeting ISG15-associated RIG-I for autophagic degradation. *EMBO J* 37:
746 351–366

747 Dunn WA, Cregg JM, Kiel JAKW, van der Klei IJ, Oku M, Sakai Y, Sibirny AA, Stasyk O V. &
748 Veenhuis M (2005) Pexophagy: the selective autophagy of peroxisomes. *Autophagy* 1: 75–
749 83

750 Dupont N, Jiang S, Pilli M, Ornatowski W, Bhattacharya D & Deretic V (2011) Autophagy-
751 based unconventional secretory pathway for extracellular delivery of IL-1β. *EMBO J* 30:
752 4701–4711

753 Ellinghaus D, Zhang H, Zeissig S, Lipinski S, Till A, Jiang T, Stade B, Bromberg Y, Ellinghaus
754 E, Keller A, *et al* (2013) Association between variants of PRDM1 and NDP52 and Crohn's
755 disease, based on exome sequencing and functional studies. *Gastroenterology* 145: 339–47

756 Ensoli B, Nakamura S, Salahuddin SZ, Biberfeld P, Larsson L, Beaver B, Wong-staal F & Gallo
757 RC (2010) AIDS-Kaposi's Sarcoma-Derived Cells Express Cytokines with Autocrine and
758 Paracrine Growth Effects. *Science (80-)* 243: 223–226

759 Ensoli B & Stürzl M (1998) Kaposi's sarcoma: a result of the interplay among inflammatory
760 cytokines, angiogenic factors and viral agents. *Cytokine Growth Factor Rev* 9: 63–83

761 Franks TM & Lykke-Andersen J (2007) TTP and BRF proteins nucleate processing body

762 formation to silence mRNAs with AU-rich elements. *Genes Dev* 21: 719–735

763 Franks TM & Lykke-Andersen J (2008) The control of mRNA decapping and P-body formation.
764 *Mol Cell* 32: 605–15

765 Fu T, Liu J, Wang Y, Xie X, Hu S & Pan L (2018) Mechanistic insights into the interactions of
766 NAP1 with the SKICH domains of NDP52 and TAX1BP1. *Proc Natl Acad Sci U S A* 115:
767 E11651–E11660

768 García-Mauriño SM, Rivero-Rodríguez F, Velázquez-Cruz A, Hernández-Vellisca M, Díaz-
769 Quintana A, De la Rosa MA & Díaz-Moreno I (2017) RNA binding protein regulation and
770 cross-talk in the control of AU-rich mRNA Fate. *Front Mol Biosci* 4: 71

771 Gjyshi O, Bottero V, Veettil MV, Dutta S, Singh VV, Chikoti L & Chandran B (2014) Kaposi's
772 sarcoma-associated herpesvirus induces Nrf2 during de novo infection of endothelial cells
773 to create a microenvironment conducive to infection. *PLoS Pathog* 10: e1004460

774 Gjyshi O, Flaherty S, Veettil MV, Johnson KE, Chandran B & Bottero V (2015) Kaposi's
775 Sarcoma-Associated Herpesvirus Induces Nrf2 Activation in Latently Infected Endothelial
776 Cells through SQSTM1 Phosphorylation and Interaction with Polyubiquitinated Keap1. *J*
777 *Virol* 89: 2268–2286

778 Green DR, Galluzzi L & Kroemer G (2011) Mitochondria and the autophagy-inflammation-cell
779 death axis in organismal aging. *Science (80-)* 333: 1109–1112

780 Guo H, Chitiprolu M, Gagnon D, Meng L, Perez-Iratxeta C, Lagace D & Gibbings D (2014)
781 Autophagy supports genomic stability by degrading retrotransposon RNA. *Nat Commun* 5:
782 5276

783 Guo L, Louis IV-S & Bohjanen PR (2018) Post-transcriptional regulation of cytokine expression
784 and signaling. *Curr Trends Immunol* 19: 33–40

785 Gurkar AU, Chu K, Raj L, Bouley R, Lee S-H, Kim Y-B, Dunn SE, Mandinova A & Lee SW
786 (2013) Identification of ROCK1 kinase as a critical regulator of Beclin1-mediated
787 autophagy during metabolic stress. *Nat Commun* 4: 2189

788 Gustafson EA & Wessel GM (2010) DEAD-box helicases: posttranslational regulation and

789 function. *Biochem Biophys Res Commun* 395: 1–6

790 Hampe J, Franke A, Rosenstiel P, Till A, Teuber M, Huse K, Albrecht M, Mayr G, De La Vega
791 FM, Briggs J, *et al* (2007) A genome-wide association scan of nonsynonymous SNPs
792 identifies a susceptibility variant for Crohn disease in ATG16L1. *Nat Genet* 39: 207–211

793 He X, Zhu Y, Zhang Y, Geng Y, Gong J, Geng J, Zhang P, Zhang X, Liu N, Peng Y, *et al* (2019)
794 RNF 34 functions in immunity and selective mitophagy by targeting MAVS for autophagic
795 degradation . *EMBO J* 38

796 Henckaerts L, Cleynen I, Brinar M, John JM, Van Steen K, Rutgeerts P & Vermeire S (2011)
797 Genetic variation in the autophagy gene ULK1 and risk of Crohn's disease. *Inflamm Bowel*
798 *Dis* 17: 1392–1397

799 Herranz N, Gallage S, Mellone M, Wuestefeld T, Klotz S, Hanley CJ, Raguz S, Acosta JC, Innes
800 AJ, Banito A, *et al* (2015) mTOR regulates MAPKAPK2 translation to control the
801 senescence-associated secretory phenotype. *Nat Cell Biol* 17: 1205–1217

802 Hubstenberger A, Courel M, Bénard M, Souquere S, Ernoult-Lange M, Chouaib R, Yi Z, Morlot
803 J-B, Munier A, Fradet M, *et al* (2017) P-Body Purification Reveals the Condensation of
804 Repressed mRNA Regulons. *Mol Cell* 68: 144-157.e5

805 Ichimura Y, Kumanomidou T, Sou Y, Mizushima T, Ezaki J, Ueno T, Kominami E, Yamane T,
806 Tanaka K & Komatsu M (2008) Structural basis for sorting mechanism of p62 in selective
807 autophagy. *J Biol Chem* 283: 22847–57

808 Jang GH, Lee J, Kim NY, Kim JH, Yeh JY, Han M, Ahn SK, Kang H & Lee M (2016)
809 Suppression of lytic replication of Kaposi's sarcoma-associated herpesvirus by autophagy
810 during initial infection in NIH 3T3 fibroblasts. *Arch Virol* 161: 595–604

811 Ji E, Kim C, Kang H, Ahn S, Jung M, Hong Y, Tak H, Lee S, Kim W & Lee EK (2019) RNA
812 Binding Protein HuR Promotes Autophagosome Formation by Regulating Expression of
813 Autophagy-Related Proteins 5, 12, and 16 in Human Hepatocellular Carcinoma Cells. *Mol*
814 *Cell Biol* 39

815 Jin S, Tian S, Luo M, Xie W, Liu T, Duan T, Wu Y & Cui J (2017) Tetherin Suppresses Type I
816 Interferon Signaling by Targeting MAVS for NDP52-Mediated Selective Autophagic

817 Degradation in Human Cells. *Mol Cell* 68: 308-322.e4

818 Jo C, Gundemir S, Pritchard S, Jin YN, Rahman I & Johnson GVW (2014) Nrf2 reduces levels
819 of phosphorylated tau protein by inducing autophagy adaptor protein NDP52. *Nat Commun*
820 5: 3496

821 Johnston BP, Pringle ES & McCormick C (2019) KSHV activates unfolded protein response
822 sensors but suppresses downstream transcriptional responses to support lytic replication.
823 *PLoS Pathog* 15

824 Kabeya Y (2000) LC3, a mammalian homologue of yeast Apg8p, is localized in autophagosome
825 membranes after processing. *EMBO J* 19: 5720–5728

826 Kayyali US, Pennella CM, Trujillo C, Villa O, Gaestel M & Hassoun PM (2002) Cytoskeletal
827 changes in hypoxic pulmonary endothelial cells are dependent on MAPK-activated protein
828 kinase MK2. *J Biol Chem* 277: 42596–42602

829 Kenific CM, Stehbens SJ, Goldsmith J, Leidal AM, Faure N, Ye J, Wittmann T & Debnath J
830 (2016) NBR 1 enables autophagy-dependent focal adhesion turnover. *J Cell Biol* 212: 577–
831 590

832 King CA (2013) Kaposi's sarcoma-associated herpesvirus kaposin B induces unique
833 monophosphorylation of STAT3 at serine 727 and MK2-mediated inactivation of the
834 STAT3 transcriptional repressor TRIM28. *J Virol* 87: 8779–91

835 Klionsky DJ, Abdalla FC, Abeliovich H, Abraham RT, Acevedo-Arozena A, Adeli K, Agholme
836 L, Agnello M, Agostinis P, Aguirre-Ghiso JA, *et al* (2012) Guidelines for the use and
837 interpretation of assays for monitoring autophagy. *Autophagy* 8: 445–544

838 Kuma A, Hatano M, Matsui M, Yamamoto A, Nakaya H, Yoshimori T, Ohsumi Y, Tokuhisa T
839 & Mizushima N (2004) The role of autophagy during the early neonatal starvation period.
840 *Nature* 432: 1032–1036

841 Lai WS & Blackshear PJ (2001) Interactions of CCCH zinc finger proteins with mRNA.
842 Tristetraprolin-mediated AU-rich element-dependent mRNA degradation can occur in the
843 absence of a poly(A) tail. *J Biol Chem* 276: 23144–23154

844 Lai WS, Carballo E, Strum JR, Kennington EA, Phillips RS & Blackshear PJ (1999) Evidence
845 that Tristetraprolin Binds to AU-Rich Elements and Promotes the Deadenylation and
846 Destabilization of Tumor Necrosis Factor Alpha mRNA. *Mol Cell Biol* 19: 4311–4323

847 Lamb CA, Yoshimori T & Tooze SA (2013) The autophagosome: Origins unknown, biogenesis
848 complex. *Nat Rev Mol Cell Biol* 14: 759–774

849 Lamkanfi M & Dixit VM (2014) Mechanisms and functions of inflammasomes. *Cell* 157: 1013–
850 1022

851 Lane BR, Liu J, Bock PJ, Schols D, Coffey MJ, Strieter RM, Polverini PJ & Markovitz DM
852 (2002) Interleukin-8 and growth-regulated oncogene alpha mediate angiogenesis in
853 Kaposi's sarcoma. *J Virol* 76: 11570–83

854 Law AHY, Lee DCW, Yuen KY, Peiris M & Lau ASY (2010) Cellular response to influenza
855 virus infection: A potential role for autophagy in CXCL10 and interferon-alpha induction.
856 *Cell Mol Immunol* 7: 263–270

857 Lazarou M, Sliter DA, Kane LA, Sarraf SA, Wang C, Burman JL, Sideris DP, Fogel AI & Youle
858 RJ (2015) The ubiquitin kinase PINK1 recruits autophagy receptors to induce mitophagy.
859 *Nature* 524: 309–314

860 Lee J-S, Li Q, Lee J-Y, Lee S-H, Jeong JH, Lee H-R, Chang H, Zhou F-C, Gao S-J, Liang C, *et*
861 *al* (2009) FLIP-mediated autophagy regulation in cell death control. *Nat Cell Biol* 11: 1355–
862 1362

863 Leidal AM, Cyr DP, Hill RJ, Lee PWK & McCormick C (2012) Subversion of autophagy by
864 Kaposi's sarcoma-associated herpesvirus impairs oncogene-induced senescence. *Cell Host*
865 *Microbe* 11: 167–180

866 Levine B, Mizushima N & Virgin HW (2011) Autophagy in immunity and inflammation. *Nature*
867 469: 323–335

868 Levine B, Sinha S & Kroemer G (2008) Bcl-2 family members: Dual regulators of apoptosis and
869 autophagy. *Autophagy* 4: 600–606

870 Liang C, Xiaofei E & Jung JU (2008) Downregulation of autophagy by herpesvirus Bcl-2

homologs. *Autophagy* 4: 268–272

Liu J & Debnath J (2016) The Evolving, Multifaceted Roles of Autophagy in Cancer. In *Advances in Cancer Research* pp 1–53. Academic Press Inc.

Luo Y, Na Z & Slavoff SA (2018) P-Bodies: Composition, Properties, and Functions. *Biochemistry* 57: 2424

Lykke-Andersen J & Wagner E (2005) Recruitment and activation of mRNA decay enzymes by two ARE-mediated decay activation domains in the proteins TTP and BRF-1. *Genes Dev* 19: 351–361

Lystad AH, Carlsson SR, de la Ballina LR, Kauffman KJ, Nag S, Yoshimori T, Melia TJ & Simonsen A (2019) Distinct functions of ATG16L1 isoforms in membrane binding and LC3B lipidation in autophagy-related processes. *Nat Cell Biol* 21: 372–383

Maitra S, Chou CF, Luber CA, Lee KY, Mann M & Chen CY (2008) The AU-rich element mRNA decay-promoting activity of BRF1 is regulated by mitogen-activated protein kinase-activated protein kinase 2. *RNA* 14: 950–959

Maiuri MC & Kroemer G (2015) Autophagy in stress and disease. *Cell Death Differ* 22: 365–366

Mauvezin C & Neufeld TP (2015) Bafilomycin A1 disrupts autophagic flux by inhibiting both V-ATPase-dependent acidification and Ca-P60A/SERCA-dependent autophagosome-lysosome fusion. *Autophagy* 11: 1437–1438

McCormick C & Ganem D (2005) The Kaposin B Protein of KSHV Activates the p38/MK2 Pathway and Stabilizes Cytokine mRNAs. *Science (80-)* 307: 739–741

Miles SA, Rezai AR, Salazar-González JF, Vander Meyden M, Stevens RH, Logan DM, Mitsuyasu RT, Taga T, Hirano T & Kishimoto T (1990) AIDS Kaposi sarcoma-derived cells produce and respond to interleukin 6. *Proc Natl Acad Sci U S A* 87: 4068–72

Mizushima N, Yoshimori T & Levine B (2010) Methods in Mammalian Autophagy Research. *Cell* 140: 313–326

Mohamud Y, Qu J, Xue YC, Liu H, Deng H & Luo H (2019) CALCOCO2/NDP52 and

898 SQSTM1/p62 differentially regulate coxsackievirus B3 propagation. *Cell Death Differ* 26:
899 1062–1076

900 Moi P, Chan K, Asunis I, Cao A & Kan YW (1994) Isolation of NF-E2-related factor 2 (Nrf2), a
901 NF-E2-like basic leucine zipper transcriptional activator that binds to the tandem NF-
902 E2/AP1 repeat of the β-globin locus control region. *Proc Natl Acad Sci U S A* 91: 9926–
903 9930

904 Morishita H & Mizushima N (2019) Diverse cellular roles of autophagy. *Annu Rev Cell Dev Biol*
905 35: 453–475

906 Morriswood B, Ryzhakov G, Puri C, Arden SD, Roberts R, Dendrou C, Kendrick-Jones J &
907 Buss F (2007) T6BP and NDP52 are myosin VI binding partners with potential roles in
908 cytokine signalling and cell adhesion. *J Cell Sci* 120: 2574–85

909 Nguyen T, Nioi P & Pickett CB (2009) The Nrf2-antioxidant response element signaling
910 pathway and its activation by oxidative stress. *J Biol Chem* 284: 13291–13295

911 Nilsen EM, Johansen F-E, Jahnsen FL, Lundin KEA, Scholz T, Brandtzaeg P & Haraldsen G
912 (1998) Cytokine profiles of cultured microvascular endothelial cells from the human
913 intestine. *Gut* 42: 635–642

914 Noda NN, Kumeta H, Nakatogawa H, Satoo K, Adachi W, Ishii J, Fujioka Y, Ohsumi Y &
915 Inagaki F (2008) Structural basis of target recognition by Atg8/LC3 during selective
916 autophagy. *Genes to Cells* 13: 1211–1218

917 Noda NN, Ohsumi Y & Inagaki F (2010) Atg8-family interacting motif crucial for selective
918 autophagy. *FEBS Lett* 584: 1379–1385

919 Orvedahl A & Levine B (2008) Viral evasion of autophagy. *Autophagy* 4: 280–285

920 Padman BS, Nguyen TN, Uoselis L, Skulsuppaisarn M, Nguyen LK & Lazarou M (2019)
921 LC3/GABARAPs drive ubiquitin-independent recruitment of Optineurin and NDP52 to
922 amplify mitophagy. *Nat Commun* 10: 1–13

923 Palanisamy V, Jakymiw A, Van Tubergen EA, D'Silva NJ & Kirkwood KL (2012) Control of
924 Cytokine mRNA Expression by RNA-binding Proteins and microRNAs. *J Dent Res* 91:

925 651–658

926 Palanisamy V, Park NJ, Wang J & Wong DT (2008) AUF1 and HuR proteins stabilize
927 interleukin-8 mRNA in human saliva. *J Dent Res* 87: 772–6

928 Park S, Buck MD, Desai C, Zhang X, Loginicheva E, Martinez J, Freeman ML, Saitoh T, Akira
929 S, Guan JL, *et al* (2016) Autophagy Genes Enhance Murine Gammaherpesvirus 68
930 Reactivation from Latency by Preventing Virus-Induced Systemic Inflammation. *Cell Host*
931 *Microbe* 19: 91–101

932 Pattingre S, Tassa A, Qu X, Garuti R, Xiao HL, Mizushima N, Packer M, Schneider MD &
933 Levine B (2005) Bcl-2 antiapoptotic proteins inhibit Beclin 1-dependent autophagy. *Cell*
934 122: 927–939

935 Peng SSY, Chen CYA, Xu N & Shyu A Bin (1998) RNA stabilization by the AU-rich element
936 binding protein, HuR, an ELAV protein. *EMBO J* 17: 3461–3470

937 Prabakaran T, Bodda C, Krapp C, Zhang B, Christensen MH, Sun C, Reinert L, Cai Y, Jensen
938 SB, Skouboe MK, *et al* (2018) Attenuation of c GAS - STING signaling is mediated by a
939 p62/ SQSTM 1-dependent autophagy pathway activated by TBK1 . *EMBO J* 37

940 Pringle ES, Robinson C-A & McCormick C (2019) Kaposi's Sarcoma-Associated Herpesvirus
941 Lytic Replication Interferes with mTORC1 Regulation of Autophagy and Viral Protein
942 Synthesis. *J Virol* 93

943 Rahman H, Qasim M, Oellerich M & Asif AR (2014) Crosstalk between Edc4 and mammalian
944 target of rapamycin complex 1 (mTORC1) signaling in mRNA decapping. *Int J Mol Sci* 15:
945 23179–95

946 Riggs CL, Kedersha N, Ivanov P & Anderson P (2020) Mammalian stress granules and P bodies
947 at a glance. *J Cell Sci* 133

948 Riva G, Barozzi P, Torelli G & Luppi M (2010) Immunological and Inflammatory Features of
949 Kaposi's Sarcom and Other Kaposi's Sarcoma-Associated Herpesvirus/Human Herpesvirus
950 8-Associated Neoplasias. *AIDS Rev* 9: 25–39

951 Rogov V, Dötsch V, Johansen T & Kirkin V (2014) Interactions between Autophagy Receptors

952 and Ubiquitin-like Proteins Form the Molecular Basis for Selective Autophagy. *Mol Cell*
953 53: 167–178

954 Rousseau S, Houle F, Landry J & Huot J (1997) P38 MAP kinase activation by vascular
955 endothelial growth factor mediates actin reorganization and cell migration in human
956 endothelial cells. *Oncogene* 15: 2169–2177

957 Sadagopan S, Sharma-Walia N, Veettil MV, Raghu H, Sivakumar R, Bottero V & Chandran B
958 (2007) Kaposi's Sarcoma-Associated Herpesvirus Induces Sustained NF-κB Activation
959 during De Novo Infection of Primary Human Dermal Microvascular Endothelial Cells That
960 Is Essential for Viral Gene Expression. *J Virol* 81: 3949–3968

961 Salahuddin S, Nakamura S, Biberfeld P, Kaplan M, Markham P, Larsson L & Gallo R (1988)
962 Angiogenic properties of Kaposi's sarcoma-derived cells after long-term culture in vitro.
963 *Science (80-)* 242: 430–433

964 Sargsyan A, Cai J, Fandino LB, Labasky ME, Forostyan T, Colosimo LK, Thompson SJ &
965 Graham TE (2015) Rapid parallel measurements of macroautophagy and mitophagy in
966 mammalian cells using a single fluorescent biosensor. *Sci Rep* 5

967 Seth RB, Sun L, Ea CK & Chen ZJ (2005) Identification and characterization of MAVS, a
968 mitochondrial antiviral signaling protein that activates NF-κB and IRF3. *Cell* 122: 669–682

969 Shaid S, Brandts CH, Serve H & Dikic I (2013) Ubiquitination and selective autophagy. *Cell*
970 *Death Differ* 20: 21–30

971 Shen L, Qi Z, Zhu Y, Song X, Xuan C, Ben P, Lan L, Luo L & Yin Z (2016) Phosphorylated
972 heat shock protein 27 promotes lipid clearance in hepatic cells through interacting with
973 STAT3 and activating autophagy. *Cell Signal* 28: 1086–1098

974 Shi CS, Shenderov K, Huang NN, Kabat J, Abu-Asab M, Fitzgerald KA, Sher A & Kehrl JH
975 (2012) Activation of autophagy by inflammatory signals limits IL-1β production by
976 targeting ubiquitinated inflammasomes for destruction. *Nat Immunol* 13: 255–263

977 Soulier J, Grollet L, Oksenhendler E, Cacoub P, Cazals-Hatem D, Babinet P, d'Agay MF,
978 Clauvel JP, Raphael M & Degos L (1995) Kaposi's sarcoma-associated herpesvirus-like
979 DNA sequences in multicentric Castleman's disease. *Blood* 86: 1276–80

980 Stallone G, Schena A, Infante B, Di Paolo S, Loverre A, Maggio G, Ranieri E, Gesualdo L,
981 Schena FP & Grandaliano G (2005) Sirolimus for Kaposi's Sarcoma in Renal-Transplant
982 Recipients. *N Engl J Med* 352: 1317–1323

983 Standart N & Weil D (2018) P-Bodies: Cytosolic Droplets for Coordinated mRNA Storage.
984 *Trends Genet* 34: 612–626

985 Staskus KA, Zhong W, Gebhard K, Herndier B, Wang H, Renne R, Beneke J, Pudney J,
986 Anderson DJ, Ganem D, *et al* (1997) Kaposi's sarcoma-associated herpesvirus gene
987 expression in endothelial (spindle) tumor cells. *J Virol* 71: 715–9

988 Sumpter R & Levine B (2011) Selective autophagy and viruses. *Autophagy* 7: 260–265

989 Tenekeci U, Poppe M, Beuerlein K, Busch J, Schmitz ML & Kracht Correspondence M (2016)
990 K63-Ubiquitylation and TRAF6 Pathways Regulate Mammalian P-Body Formation and
991 mRNA Decapping. *Mol Cell* 62: 943–957

992 Thoreen CC, Kang SA, Won Chang J, Liu Q, Zhang J, Gao Y, Reichling LJ, Sim T, Sabatini DM
993 & Gray NS (2009) An ATP-competitive Mammalian Target of Rapamycin Inhibitor
994 Reveals Rapamycin-resistant Functions of mTORC1. *J Biol Chem* 284: 8023-32

995 Till A, Lipinski S, Ellinghaus D, Mayr G, Subramani S, Rosenstiel P & Franke A (2013)
996 Autophagy receptor CALCOCO2/NDP52 takes center stage in Crohn disease. *Autophagy* 9:
997 1256–7

998 Tran H, Maurer F & Nagamine Y (2003) Stabilization of Urokinase and Urokinase Receptor
999 mRNAs by HuR Is Linked to Its Cytoplasmic Accumulation Induced by Activated
1000 Mitogen-Activated Protein Kinase-Activated Protein Kinase 2. *Mol Cell Biol* 23: 7177–
1001 7188

1002 Tripathi DN, Zhang J, Jing J, Dere R & Walker CL (2016) A new role for ATM in selective
1003 autophagy of peroxisomes (pexophagy). *Autophagy* 12: 711–712

1004 Turakhiya A, Meyer SR, Marincola G, Böhm S, Vanselow JT, Schlosser A, Hofmann K &
1005 Buchberger A (2018) ZFAND1 Recruits p97 and the 26S Proteasome to Promote the
1006 Clearance of Arsenite-Induced Stress Granules. *Mol Cell* 70: 906-919.e7

1007 Verlhac P, Gré IP, Viret C & Faure M (2015) Autophagy Receptor NDP52 Regulates Pathogen-
1008 Containing Autophagosome Maturation. *Cell Host Microbe* 17: 515–525

1009 Vescovo T, Pagni B, Piacentini M, Fimia GM & Antonioli M (2020) Regulation of Autophagy in
1010 Cells Infected With Oncogenic Human Viruses and Its Impact on Cancer Development.
1011 *Front Cell Dev Biol* 8

1012 Vindry C, Marnef A, Broomhead H, Twyffels L, Ozgur S, Stoecklin G, Llorian M, Smith CW,
1013 Mata J, Weil D, *et al* (2017) Dual RNA Processing Roles of Pat1b via Cytoplasmic Lsm1-7
1014 and Nuclear Lsm2-8 Complexes. *Cell Rep* 20: 1187–1200

1015 Wang L, Howell MEA, Sparks-Wallace A, Hawkins C, Nicksic CA, Kohne C, Hall KH,
1016 Moorman JP, Yao ZQ & Ning S (2019) p62-mediated Selective autophagy endows virus-
1017 transformed cells with insusceptibility to DNA damage under oxidative stress. *PLoS Pathog*
1018 15

1019 Wei Y, An Z, Zou Z, Sumpter R, Su M, Zang X, Sinha S, Gaestel M & Levine B (2015) The
1020 stress-responsive kinases MAPKAPK2/MAPKAPK3 activate starvation-induced autophagy
1021 through Beclin 1 phosphorylation. *Elife* 4

1022 Wei Y, Pattingre S, Sinha S, Bassik M & Levine B (2008) JNK1-Mediated Phosphorylation of
1023 Bcl-2 Regulates Starvation-Induced Autophagy. *Mol Cell* 30: 678–688

1024 Wen KW & Damania B (2010) Kaposi sarcoma-associated herpesvirus (KSHV): molecular
1025 biology and oncogenesis. *Cancer Lett* 289: 140–50

1026 Wu WKK, Coffelt SB, Cho CH, Wang XJ, Lee CW, Chan FKL, Yu J & Sung JJY (2012) The
1027 autophagic paradox in cancer therapy. *Oncogene* 31: 939–953

1028 Wu Y, Jin S, Liu Q, Zhang Y, Ma L, Zhao Z, Yang S, Li YP & Cui J (2020) Selective autophagy
1029 controls the stability of transcription factor IRF3 to balance type I interferon production and
1030 immune suppression. *Autophagy* In press

1031 Xie X, Li F, Wang Y, Wang Y, Lin Z, Cheng X, Liu J, Chen C & Pan L (2015) Molecular basis
1032 of ubiquitin recognition by the autophagy receptor CALCOCO2. *Autophagy* 11: 1775–1789

1033 Yang Q, Liu TT, Lin H, Zhang M, Wei J, Luo WW, Hu YH, Zhong B, Hu MM & Shu HB

1034 (2017) TRIM32-TAX1BP1-dependent selective autophagic degradation of TRIF negatively
1035 regulates TLR3/4-mediated innate immune responses. *PLoS Pathog* 13

1036 Yao Z & Klionsky DJ (2016) An unconventional pathway for mitochondrial protein degradation.
1037 *Autophagy* 12: 1971–1972

1038 Yoo J, Kang J, Lee HN, Aguilar B, Kafka D, Lee S, Choi I, Lee J, Ramu S, Haas J, *et al* (2010)
1039 Kaposin-B enhances the PROX1 mRNA stability during lymphatic reprogramming of
1040 vascular endothelial cells by Kaposi's sarcoma herpes virus. *PLoS Pathog* 6: e1001046

1041 Yoon J-H, Choi E-J & Parker R (2010) Dcp2 phosphorylation by Ste20 modulates stress granule
1042 assembly and mRNA decay in Saccharomyces cerevisiae. *J Cell Biol* 189: 813–27

1043 Youn JY, Dunham WH, Hong SJ, Knight JDR, Bashkurov M, Chen GI, Bagci H, Rathod B,
1044 MacLeod G, Eng SWM, *et al* (2018) High-Density Proximity Mapping Reveals the
1045 Subcellular Organization of mRNA-Associated Granules and Bodies. *Mol Cell* 69: 517-
1046 532.e11

1047 Young ARJ, Narita M, Ferreira M, Kirschner K, Sadaie M, Darot JFJ, Tavaré S, Arakawa S,
1048 Shimizu S, Watt FM, *et al* (2009) Autophagy mediates the mitotic senescence transition.
1049 *Genes Dev* 23: 798–803

1050 Zaffagnini G & Martens S (2016) Mechanisms of Selective Autophagy. *J Mol Biol* 428: 1714–
1051 1724

1052 Zhang M, Kenny SJ, Ge L, Xu K & Schekman R (2015) Translocation of interleukin-1β into a
1053 vesicle intermediate in autophagy-mediated secretion. *Elife* 4

1054

1055 **Figure Legends**

1056 **Figure 1: Kaposin B increases autophagic flux.** Primary human umbilical vein endothelial
1057 cells (HUVECs) were transduced with recombinant lentiviruses expressing either Kaposin B
1058 (KapB) or an empty vector control and selected with blasticidin (5 µg/mL). A: Cells were treated
1059 with bafilomycin A1 (10 nM) or a vehicle control (DMSO) for the indicated times prior to
1060 harvest in 2x Laemmli buffer. Protein lysates were resolved by SDS-PAGE and immunoblot was

1061 performed for LC3. Samples were quantified by normalizing LC3-II protein levels to the total
1062 protein in each lane using Image Lab (Biorad) and then to their relative 0 h time point. Results
1063 were plotted in GraphPad and a linear regression statistical test was performed with a Šidák's
1064 multiple comparison test, ±SEM; n=3, *=P<0.01. B: Cells were treated as above for 30 min prior
1065 to fixation in methanol. Immunofluorescence was performed for LC3 (white) and DAPI (nuclei,
1066 blue). Scale bar=20 µm. Total LC3 area per field was quantified by identifying LC3 puncta using
1067 CellProfiler and normalizing to the number of nuclei. Results were plotted in GraphPad, a 2-way
1068 ANOVA was performed, ±SEM; n=3, *=P<0.05. C: HUVECs were transduced with lentiviruses
1069 expressing KapB or an empty vector control, selected with blasticidin (5 µg/mL) for 48 h, and
1070 recovered for 24 h in antibiotic-free media before fixation in 2.5% glutaraldehyde. Thin sections
1071 were cut at approximately 100 nm and samples were observed on a JEOL JEM 1230
1072 Transmission Electron Microscope at 80kV. Scale bars are indicated on the image.

1073 **Figure 2: KapB-mediated PB disassembly requires canonical autophagy machinery.** A:
1074 HUVECs were sequentially transduced: first with recombinant lentiviruses expressing either
1075 shRNAs targeting Atg5 (shAtg5) or a non-targeting control (NS) and selected with puromycin (1
1076 µg/mL), and second, with either KapB or an empty vector control and selected with blasticidin (5
1077 µg/mL). Coverslips were fixed in 4% v/v paraformaldehyde, permeabilized in 0.1% Triton X-
1078 100, and immunostained for the PB-resident protein Hedls (white) and nuclei (DAPI). Scale
1079 bar=20 µm. B: Hedls puncta were quantified using CellProfiler and normalized to the number of
1080 nuclei, results were plotted in GraphPad and a 2-way ANOVA was performed, with a Šidák's
1081 multiple comparison test, ±SEM; n=4, *=P<0.05. C: In parallel, cells treated as in A were
1082 harvested in 2x Laemmli buffer and resolved by SDS-PAGE, immunoblot was performed for
1083 Atg5 and LC3. Samples were quantified by normalizing Atg5 protein levels to the total protein in
1084 each lane using Image Lab (Biorad) and then to Vector NS. Results were plotted in GraphPad, a
1085 2-way ANOVA was performed, ±SEM; n=3, ***=P<0.001. D: Atg5 +/+ and -/- MEFs were
1086 transduced with recombinant viruses expressing KapB or an empty vector control and selected
1087 and processed as in A. E: Hedls puncta quantification and statistical analysis was performed as
1088 described in B. ±SEM; n=3, *=P<0.05, **=P<0.01.

1089 **Figure 3: Chemical inhibition of autophagy reverses KapB-mediated PB disassembly.**
1090 HUVECs were transduced with recombinant lentiviruses expressing either KapB or an empty

1091 vector control and selected with blasticidin (5 µg/mL). A: Cells were treated with DMSO or
1092 bafilomycin A1 (10 nM) for 30 min before being fixed in 4% paraformaldehyde and
1093 permeabilized in 0.1% Triton X-100. Immunofluorescence was performed for Hedls (PBs, white)
1094 and DAPI (nuclei, blue). Scale bar=20 µm. B: Hedls puncta were counted using CellProfiler and
1095 normalized to the number of nuclei and the Vector DMSO control, results were plotted in
1096 GraphPad and a 2-way ANOVA was performed, performed with a Šidák's multiple comparison
1097 test, ±SEM; n=3, *=P<0.05. C: Cells were treated with DMSO, Torin (250 nM) or chloroquine
1098 (CQ, 25 µM) prior to harvest in 2x Laemmli buffer. Samples were resolved by SDS-PAGE and
1099 immunoblot was performed for Dcp1a, Xrn1, EDC4/Hedls (PB resident proteins) and p62
1100 (autophagy marker). Samples were quantified by normalizing Dcp1a protein levels to the total
1101 protein in each lane using Image Lab (Biorad) and then to the Vector DMSO control. Results
1102 were plotted in GraphPad and a 2-way ANOVA was performed, ±SEM; n=3, *=P<0.1.

1103 **Figure 4: KapB-mediated ARE-mRNA reporter expression requires autophagy.** A:
1104 HUVECs were transduced with recombinant lentiviruses expressing either KapB or an empty
1105 vector control and selected with blasticidin (5 µg/mL). Cells were treated with LPS (1 µg/mL)
1106 for the indicated times prior to lysis for total RNA. Transcript levels were quantified by qPCR
1107 and normalized to 18S as a reference gene. Data is represented as the fold change in target
1108 transcript expression relative to the untreated vector control and was quantified using the ΔΔCq
1109 method. For IL-6 and CXCL8 ±SEM; n=3, ****=P<0.0001. For GM-CSF and TNF bars indicate
1110 ranges, n=2. B: HeLa Tet-Off cells were transduced with recombinant lentiviruses expressing
1111 either shRNAs targeting Atg5 (shAtg5) or a non-targeting control (NS) and selected with
1112 puromycin (1 µg/mL). These cells were then co-transfected with expression plasmids for a
1113 degradation-sensitive firefly luciferase plasmid (pTRE-Fluc-ARE), a stable renilla luciferase
1114 plasmid (pTRE-Rluc), and KapB or an empty vector control. 36 h post transfection, doxycycline
1115 (Dox) was added to halt reporter gene transcription; 12 h after Dox addition, lysates were
1116 harvested in passive lysis buffer (Promega). Luciferase activity for both firefly and renilla was
1117 analyzed using the Dual-Luciferase Reporter Assay (Promega) and normalized (firefly/renilla)
1118 relative luciferase was calculated in relative light units (RLUs). Results were plotted using
1119 GraphPad, an unpaired t-test was performed, ±SEM; n=3, *=P<0.05, **=P<0.01. In B,
1120 bafilomycin (10 nM) was added at the same time as Dox. Results were plotted in GraphPad and a
1121 Student's t-test was performed, ±SEM; n=3, *=P<0.05, **=P<0.01.

1122 **Figure 5: Canonical autophagy is not required for MK2-mediated PB disassembly.** A:
1123 HUVECs were transduced with recombinant lentiviruses expressing either constitutively active
1124 MK2 (MK2EE) or an empty vector control and selected with blasticidin (5 µg/mL) for 48 h.
1125 Cells were treated with DMSO or bafilomycin A1 (10 nM) for 30 min before being fixed in
1126 methanol. Immunofluorescence was performed for LC3 (autophagosomes, white) and DAPI
1127 (nuclei, blue). Scale bar=20 µm. Total LC3 area per field was quantified by identifying LC3
1128 puncta using CellProfiler and normalizing to the number of nuclei. Results were plotted in
1129 GraphPad and a 2-way ANOVA was performed, with a Šidák's multiple comparison test, ±SEM
1130 n=3; *=P<0.05. B: HUVECs were sequentially transduced: first with recombinant lentiviruses
1131 expressing either shRNAs targeting Atg5 (shAtg5) or a non-targeting control (NS) and selected
1132 with puromycin (1 µg/mL), and second, with either MK2EE or an empty vector control and
1133 selected with blasticidin (5 µg/mL). Coverslips were fixed in 4% v/v paraformaldehyde,
1134 permeabilized in 0.1% Triton X-100 v/v, and immunostained for the PB-resident protein Hedls
1135 (PBs, white) and DAPI (nuclei, blue). Scale bar=20 µm. Hedls puncta were counted using
1136 CellProfiler and normalized to the number of nuclei, results were plotted in GraphPad and a 2-
1137 way ANOVA was performed, with a Šidák's multiple comparison test, ±SEM n=4; *=P<0.05. C:
1138 HeLa Tet-Off cells were transduced with recombinant lentiviruses as in Figure 4. These cells
1139 were then co-transfected with expression plasmids for pTRE-Fluc-ARE, pTRE-Rluc, and
1140 MK2EE or an empty vector control. The Dox addition, lysis, and measurement of luciferase
1141 RLUs was performed as in Figure 4. Results were plotted using GraphPad, a Student's t-test was
1142 performed, ±SEM, n=4; *=P<0.05.

1143 **Figure 6. KapB-mediated PB disassembly and ARE-mRNA stability require the selective**
1144 **autophagy receptor NDP52.** A: HUVECs were sequentially transduced with recombinant
1145 lentivirus expressing KapB or an empty vector control and selected with blasticidin (5 µg/mL),
1146 and second with shRNAs targeting NDP52, OPTN, p62 or a non-targeting control (NS) and
1147 selected with puromycin (1 µg/mL). Coverslips were fixed in 4% v/v paraformaldehyde,
1148 permeabilized in 0.1% Triton X-100 and immunostained for Hedls (PBs; white), DAPI (nuclei,
1149 blue). Scale bar=20 µm. B: Cells were imaged and the mean number of Hedls puncta per cell
1150 were quantified using CellProfiler. Data were plotted in GraphPad as the mean number of Hedls
1151 puncta per cell per condition ± SEM; n=3. A 2-way ANOVA was performed with a Šidák's
1152 multiple comparison test; * = P<0.05 **= P<0.01. C: HeLa Tet-Off cells were transduced with

1153 recombinant lentivirus expressing shRNAs targeting NDP52, OPTN, p62 or a NS control and
1154 selected with puromycin (1µg/mL). Cells were co-transfected, treated with Dox and luciferase
1155 activity was recorded and analyzed as in Figure 4. Data were plotted in GraphPad as the mean
1156 fold change in the relative luciferase activity of each condition compared to vector NS or KapB
1157 NS; n=4. An unpaired t-test was performed; * = P<0.05 **= P<0.01.

1158 **Figure 7. MK2EE-mediated PB disassembly and ARE-mRNA stabilization does not**
1159 **require NDP52.** A: HUVECs were sequentially transduced with recombinant lentivirus
1160 expressing shRNAs targeting NDP52, OPTN, p62 or a non-targeting control (NS) and selected
1161 with puromycin (1 µg/mL) and second with recombinant lentivirus expressing constitutively
1162 active MK2EE or an empty vector control and selected with blasticidin (5 µg/mL). Coverslips
1163 were fixed in 4% v/v paraformaldehyde, permeabilized in 0.1% Triton X-100, and
1164 immunostained for Hedls (PBs, white) and DAPI (nuclei, blue). Scale bar = 20 µm. B: Cells
1165 were imaged and the mean number of Hedls puncta per cell were quantified using CellProfiler.
1166 Data were plotted in GraphPad as the mean number of Hedls puncta per cell per condition ±
1167 SEM; n=3. C: HeLa Tet-Off cells were transduced with recombinant lentivirus expressing
1168 shRNAs targeting NDP52, OPTN, p62 or a NS control and selected with puromycin (1µg/mL).
1169 Cells were were co-transfected with expression plasmids for a degradation-sensitive firefly
1170 luciferase plasmid (pTRE-Fluc-ARE), a stable renilla luciferase plasmid (pTRE-Rluc), and
1171 MK2EE or an empty vector control. Cells were treated with Dox and luciferase activity was
1172 recorded and analyzed as in Figure 4. Data is plotted in GraphPad as the mean fold change in the
1173 relative luciferase activity of each condition compared to vector NS or MK2EE NS; n=3. An
1174 unpaired t-test was performed; * = P<0.05 **= P<0.01.

1175 **Figure 8. KapB-mediated PB disassembly is restored by wild-type NDP52 but not by**
1176 **ubiquitin-binding domain or LC3-interacting region mutants.** A: Schematic of NDP52.
1177 NDP52 contains the following domains and interacting regions: SKICH domain (SKIP-carboxyl
1178 homology domain), CLIR (non-canonical LC3-interaction motif), coiled-coil domain, GALB
1179 (galectin binding domain) ZF1 & ZF2 (zinc finger domains). Known mutations that disrupt
1180 NDP52 function include: V136S which prevents binding to LC3-C and C443K which prevents
1181 binding to ubiquitin. B: HUVECs were transduced first with recombinant lentivirus expressing
1182 shDNP52 targeting the 3'-UTR of NDP52 or a NS control and selected with blasticidin (5

1183 µg/mL), and second, transduced with either vector or KapB and one of the following: mCherry
1184 control (mCh), RFP-NDP52 wt, mCh-NDP52 C443K or mCh-NDP52 V136S/C443K.
1185 Coverslips were fixed with 4% v/v paraformaldehyde, permeabilized with 0.1% Triton X-100,
1186 and were immunostained with Hedls (PBs, green). Scale bar=20 µm. C: In parallel with A,
1187 HUVECs treated as in A were immunostained using WGA (to denote cellular membranes),
1188 DAPI (nuclei) and Hedls (green). Cells were imaged and the mean number of PBs per cell were
1189 quantified using CellProfiler. Results were plotted in GraphPad and a 2-way ANOVA was
1190 performed with a Šidák's multiple comparison test, ±SEM n=3; *=P<0.05, **=P<0.01.

1191 **Figure 9: Model of NDP52-dependent PB disassembly elicited by KapB.** Under normal
1192 conditions, the cytoplasm of all cells contain PBs, granules comprised of RNA and RNA decay
1193 proteins that are visible by immunofluorescent microscopy. When KapB is expressed,
1194 microscopically visible PBs are lost but can reform after overexpression of Dcp1a-GFP or after
1195 stress-induced translation shutoff. PB disassembly elicited by KapB depends on the selective
1196 autophagy receptor, NDP52. KapB expression also decreases the steady-state level of the PB
1197 protein, Dcp1a, but does not markedly alter the levels of other PB proteins like DDX6,
1198 ECD4/Hedls, or Xrn1. Dcp1a has been shown to be modified by phosphorylation and
1199 ubiquitination (Tenekeci *et al*, 2016; Aizer *et al*, 2013; Chiang *et al*, 2013) and these
1200 modifications alter PB formation and function. These data lead us to propose the following
1201 model. KapB expression leads to an as yet undetermined post-translational modification that
1202 promotes its recognition by the selective autophagy receptor, NDP52. Simultaneous binding of
1203 NDP52 to modified Dcp1a (or another unidentified PB protein) and to LC3 on the nascent
1204 phagophore recruit Dcp1a to the autophagosome for degradation. The loss of Dcp1a or another
1205 PB protein via selective autophagy leads to PB disassembly but does not prevent *de novo* PB
1206 assembly under stress, even during KapB expression.

1207 DDX6/Rck: RNA helicase, EDC4/Hedls: decapping co-factor, Dcp2: catalytic component of
1208 decapping machinery, Dcp1a: decapping co-factor, ECD3: decapping enhancer, Xrn1: 3'-5'
1209 exonuclease.

1210

1211 Table 1: Antibodies

Antibody	Species	Vendor/Catalogue #	Application	Dilution
Hedls	Mouse	Santa Cruz sc-8418	Immunofluorescence Immunoblot	1:1000 1:1000
KapB	Rabbit	A generous gift from Don Ganem	Immunofluorescence	1:1000
NDP52	Rabbit	CST 60732	Immunoblot	1:1000
p62	Rabbit	CST 7695	Immunoblot	1:1000
Dcp1a	Mouse	CST 15365	Immunoblot	1:500
MK2	Rabbit	CST 12155	Immunofluorescence	1:1000
Total Brf1	Rabbit	CST 2119	Immunoblot	1:1000
Phospho-Brf1 (S92)	Rabbit	Abcam ab79191	Immunoblot	1:1000
LC3B	Rabbit	CST 2775	Immunofluorescence Immunoblot	1:200 1:1000
Atg5	Rabbit	CST 2630	Immunoblot	1:1000
OPTN	Rabbit	Abcam ab23666	Immunoblot	1:1000
Xrn1	Rabbit	Abcam ab231197	Immunoblot	1:1000
VCP	Rabbit	CST 2649	Immunoblot	1:1000
NBR1	Rabbit	CST 9891	Immunoblot	1:1000

1212

1213 Table 2: shRNA target sequences

shRNA target	shRNA sequence 5'→3'	Region
Non-targeting (NS)	AGCACAAGCTGGAGTACAACTA	
Atg5	CTTTGATAATGAACAGTGAGA	CDS
NDP52(1)	GAGCTGCTTCAACTGAAAGAA	CDS
NDP52(2)	GACTTGCCTATGGAAACCCAT	CDS
NDP52(3)	CCCTTTGTGAACTAAGTTCAA	3'-UTR
NDP52(4)	CCTGACTTGATACTAAGTGAT	3'-UTR
Optineurin (1)	GCACGGCATTGTCTAAATATA	CDS
Optineurin (2)	GCCATGAAGCTAAATAATCAA	CDS
p62	CCGAATCTACATTAAAGAGAA	CDS
NBR1 (1)	GCCAGGAACCAAGTTTATCAA	CDS
NBR1 (2)	CCATCCTACAATATCTGTGAA	CDS
VCP (1)	ACCGTCCCAATCGGTTAATTG	CDS
VCP (2)	AGATCCGTCGAGATCACTTTG	CDS

1214

1215 Table 3: qPCR primers

Primer	Primer Sequence
18S - Forward	5' TTCGAACGTCTGCCCTATCAA 3'
18S - Reverse	5' GATGTGGTAGCCGTTTCTCAGG 3'

IL-6 - Forward	5’ GAAGCTCTATCTCGCCTCCA 3’
IL-6 - Reverse	5’ TTTTCTGCCAGTGCCTCTTT 3’
CXCL8 - Forward	5’ AAATCTGGCAACCCTAGTCTG 3’
CXCL8 - Reverse	5’ GTGAGGTAAGATGGTGGCTAAT 3’
TNF - Forward	5’ TCGAACCCCGAGTGACAA 3’
TNF - Reverse	5’ AGCTGCCCCTCAGCTTG 3’
GM-CSF - Forward	5’ AAATGTTTGACCTCCAGGAGC C 3’
GM-CSF - Reverse	5’ ATCTGGGTTGCACAGGAAGTT 3’

1216

1217 Table 4: Cloning primers

Primer	**Primer Sequence**
NDP52 C443K & C443K/V136S BamHI-Forward	5’ TAAGCAGGATCCGCCACCATGGTGAGCAAG 3’
NDP52 C443K & C443K/V136S EcoRI-Reverse	5’ TAAGCAGAATTCCAGAGAGAGTGTTTGAACACGT 3’

1218

1219 Table 5: Plasmids

Plasmid	**Use**	**Source**	**Mammalian Selection**
pBMN mCh NDP52 C443K	UBD mutant	Addgene #119685	N/A
pBMN mCh NDP52 C443K V136S	UBD/LIR mutant	Addgene #119686	N/A
RFP-NDP52	Overexpression	Dr. Andreas Till (University Hospital of Bonn)	N/A
pcDNA 3.1 (+)	Empty Vector Control	Invitrogen V79020	N/A
pcDNA KapB BCBL1	ARE-mRNA stability	(Corcoran *et al*, 2015)	N/A
pcDNA FLAG-MK2EE	ARE-mRNA stability	(Corcoran *et al*, 2015)	N/A
pLKO.1-TRC	shRNA expression	Addgene #10878	Puromycin
pLKO.1-blast	shRNA expression	Addgene #26655	Blasticidin
pLJM1	Empty Vector Control	(Johnston *et al*, 2019)	Blasticidin/ Puromycin
pLJM1 KapB (pulmonary KS)	Overexpression	Cloned from pBMNIP-KapB (Corcoran *et al*, 2015) into pLJM1-BSD	Blasticidin

Plasmid	Use	Source	Mammalian Selection
pLJM1 mCh	Overexpression Control	Craig McCormick (Dalhousie University)	Blasticidin
pLJM1 FLAG-MK2EE	Overexpression	Cloned into pLJM1 using BamHI and EcoRI from pBMN FLAG-MK2EE (Corcoran *et al*, 2015)	Blasticidin/ Puromycin
pLJM1 RFP-NDP52	Overexpression	Cloned into pLJM1 using NheI and BamHI from RFP-NDP52	Puromycin
pLJM1 mCh-NDP52 C443K	Overexpression	Cloned into pLJM1 from Addgene #119685 using the primers listed in Table 4	Blasticidin/ Puromycin
pLJM1 mCh-NDP52 C443K V136S	Overexpression	Cloned into pLJM1 from Addgene #119686 using the primers listed in Table 4	Blasticidin/ Puromycin
pMD2.G	Lentivirus generation	Addgene #12259	N/A
psPAX2	Lentivirus generation	Addgene #12260	N/A
pTRE2 Firefly Luciferase-ARE	ARE-mRNA stability	(Corcoran *et al*, 2011)	N/A
pTRE2-Renilla Luciferase	ARE-mRNA stability	(Corcoran *et al*, 2011)	N/A

1220

1221 Table 6: Drugs

Drug	Vendor/Catalogue #	Concentration
Torin1	Sigma-Aldrich 475991	250 nM
Bafilomycin A1	Sigma-Aldrich B1793	10 nM
Chloroquine	Sigma-Aldrich C6628	25 µM
MG-132	Selleckchem S2619	5 µM
LPS	Sigma-Aldrich L3129	1 µg/mL
Sodium Arsenite	Sigma-Aldrich 1.06277	0.25 mM
Doxycycline	Sigma-Aldrich D9891	1 µg/mL

1222

1223

1224 **Supplementary Figure Legends**

1225 **Figure S1: KapB expression promotes PB disassembly but does not prevent PB assembly.**
1226 HeLa cells expressing a doxycycline-inducible GFP-Dcp1a were used to determine whether
1227 KapB prevented granule assembly or promoted disassembly. A: HeLa cells were transfected with
1228 either KapB or an empty vector control prior to inducing expression of GFP-Dcp1a with

1229 doxycycline (1 µg/mL). Cells were fixed 12 h post-induction and immunostained for Hedls (PBs,
1230 red) and KapB (blue). PBs were visually analyzed. Scale bar=20 µm. A timeline of the
1231 experimental conditions is shown. B: GFP-Dcp1a expression was induced with doxycycline (1
1232 µg/mL) in HeLa cells prior to transfection with either KapB or an empty vector control. Cells
1233 were fixed 12 h post-transfection and immunostained for Hedls (PBs, red) and KapB (blue). PBs
1234 were visually analyzed. Scale bar=20 µm. A timeline of the experimental conditions is shown. C:
1235 HUVECs were transduced with recombinant lentiviruses expressing either KapB or an empty
1236 vector control and selected with blasticidin (5 µg/mL). Cells were treated with sodium arsenite (5
1237 µM) to promote PB assembly, or a vehicle control for 30 min prior to fixation in 4% v/v
1238 paraformaldehyde. Samples were permeabilized in 0.1% Triton X-100 and immunostained with
1239 Hedls (red, PBs), KapB (green), and DAPI (nuclei). Scale bar=20 µm.

1240 **Figure S2: Western blots validating shRNA silencing and knockout cell lines used in this**
1241 **study.** All samples were lysed in 2x Laemmli buffer and resolved by SDS-PAGE before
1242 immunoblotting with the indicated antibodies. A: Representative western blot of LC3 in Atg5
1243 +/+ (WT) and -/- (KO) MEFs. B: Representative western blot of HUVECs transduced with either
1244 an shRNA targeting Atg5 or a non-targeting control (NS) and selected with puromycin (1
1245 µg/mL), then transduced with an empty vector control or MK2EE and selected with blasticidin
1246 (5 µg/mL). C: Representative western blot of HUVECs transduced with shRNAs targeting
1247 NDP52, OPTN, p62, VCP, NBR1, or a non-targeting control (NS) and selected with puromycin
1248 (1 µg/mL), then transduced with an empty vector control or KapB and selected with blasticidin
1249 (5 µg/mL). VCP knockdowns were lethal, total protein is shown to reflect this. D: Representative
1250 western blot of HeLas transduced with shRNAs targeting NDP52, OPTN, p62, or a non-targeting
1251 control (NS) and selected with puromycin (1 µg/mL), then transfected with an empty vector
1252 control or KapB. E: Representative western blot of HeLas transduced with shRNAs targeting
1253 NDP52, OPTN, p62, or a non-targeting control (NS) and selected with puromycin (1 µg/mL),
1254 then transduced with an empty vector control or MK2EE and selected with blasticidin (5
1255 µg/mL). F: Representative western blot of HUVECs transduced with an shRNA targeting the
1256 3'UTR of NDP52 or a non-targeting control (NS) and selected with puromycin (1 µg/mL), then
1257 co-transduced with an empty vector control and mCherry (mCh) or KapB and mCh.

1258 **Figure S3: Proteasome inhibition does not increase steady-state levels of PB proteins.** A:
1259 HUVECs were treated with DMSO, Torin (250 nM) or BafA1 (10 nM) for 4 h prior to harvest.
1260 Samples were lysed in 2x Laemmli buffer and resolved by SDS-PAGE before immunoblotting
1261 with Xrn1, EDC4/Hedls, Dcp1a, and DDX6. Samples were quantified by normalizing the PB
1262 resident protein levels to the total protein in each lane and then the DMSO control using
1263 ImageLab (Biorad). Results were plotted in GraphPad and a one-way ANOVA was performed
1264 ±SEM; n=3, *=P<0.1. B: HUVECs were treated with DMSO, Torin (250 nM), BafA1 (10 nM),
1265 CQ (25 µM), a combination of Torin and BafA1, or MG-132 (5 µM) for 4 h prior to harvest.
1266 Samples were lysed in 2x Laemmli buffer and resolved by SDS-PAGE before immunoblotting
1267 with Dcp1a, two immunoblots are shown. Samples were quantified by normalizing Dcp1a
1268 protein levels to the total protein in each lane and then the DMSO control using ImageLab
1269 (Biorad). Results were plotted in GraphPad.

1270 **Figure S4: Genetic knockdown of OPTN and p62 do not restore PBs in KapB- or MK2EE-**
1271 **expressing cells.** A: HUVECs were transduced with shRNAs targeting OPTN, p62, or a non-
1272 targeting control (NS) and selected with puromycin (1 µg/mL), then transduced with an empty
1273 vector control or KapB and selected with blasticidin (5 µg/mL). Coverslips were fixed in 4% v/v
1274 paraformaldehyde, permeabilized in 0.1% Triton X-100 and immunostained for Hedls (PBs;
1275 white), DAPI (nuclei, blue). Scale bar=20 µm. B: HUVECs were transduced with shRNAs as in
1276 A and then transduced with an empty vector control or MK2EE and selected with blasticidin (5
1277 µg/mL). Coverslips were fixed, permeabilized, and immunostained as in A. Scale bar=20 µm.

1278 **Figure S5: MK2EE expression but not KapB expression induces phosphorylation of BRF1**.
1279 A: HUVECs were transduced with KapB, MK2EE, or an empty vector control and selected with
1280 blasticidin (5 µg/mL). Cells were treated with Torin (250 nM) or a DMSO control for 2 h prior to
1281 harvest. Samples were lysed in 2x Laemmli and resolved by SDS-PAGE before immunoblotting
1282 with either phospho-BRF1 (S92) or Total BRF1

1283 **Figure S6: NDP52 overexpression in control HUVECs.** A: HUVECs were transduced first
1284 with recombinant lentivirus expressing shDNP52 targeting the 3'-UTR of NDP52 or a NS
1285 control and selected with blasticidin (5 µg/mL), and second, transduced with either vector or
1286 KapB and one of the following: mCherry control (mCh), RFP-NDP52 wt, mCh-NDP52 C443K
1287 or mCh-NDP52 V136S/C443K. Coverslips were fixed with 4% v/v paraformaldehyde,

1288 permeabilized with 0.1% Triton X-100, and were immunostained with Hedls (PBs, green). Scale
1289 bar=20 µm. B: In parallel with A, HUVECs treated as in A were immunostained using WGA (to
1290 denote cellular membranes), DAPI (nuclei) and Hedls (green). Cells were imaged and the mean
1291 number of PBs per cell were quantified using CellProfiler. Results were plotted in GraphPad.

1292

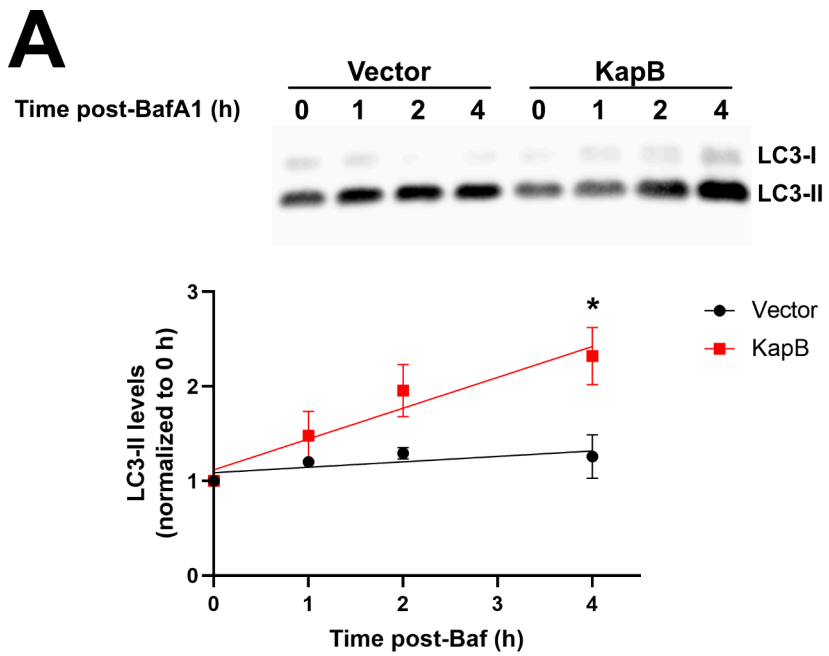
A
Vector
KapB
Time post-BafA1 (h)
0 1 2 4 0 1 2 4
LC3-I
LC3-II
LC3-II levels (normalized to 0 h)
Time post-Baf (h)
Vector
KapB
*

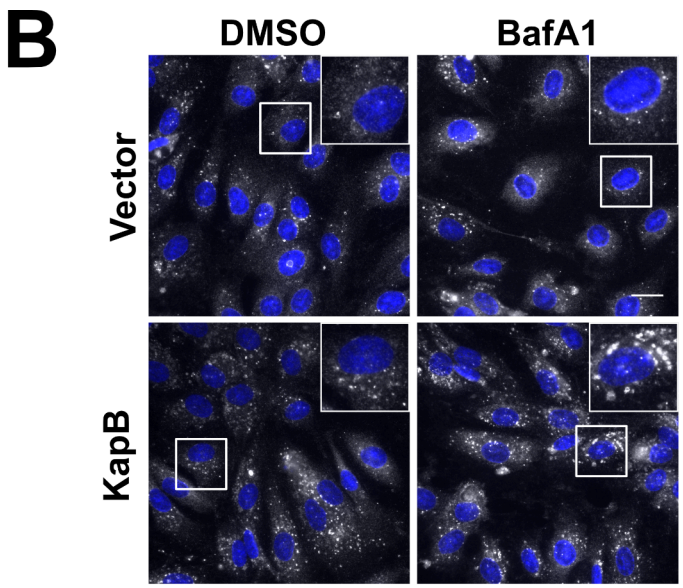
B
DMSO
BafA1
Vector
KapB

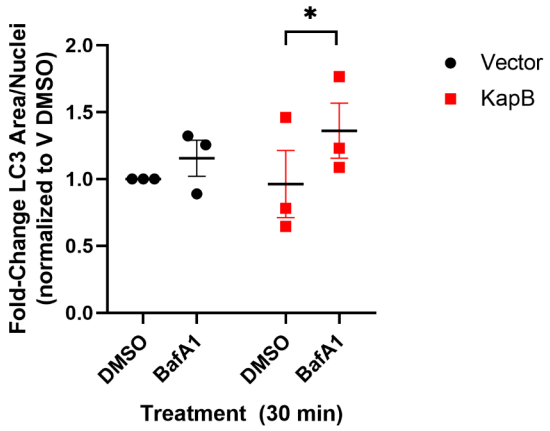
Fold-Change LC3 Area/Nuclei (normalized to V DMSO)
Treatment (30 min)
DMSO
BafA1
DMSO
BafA1
Vector
KapB
*

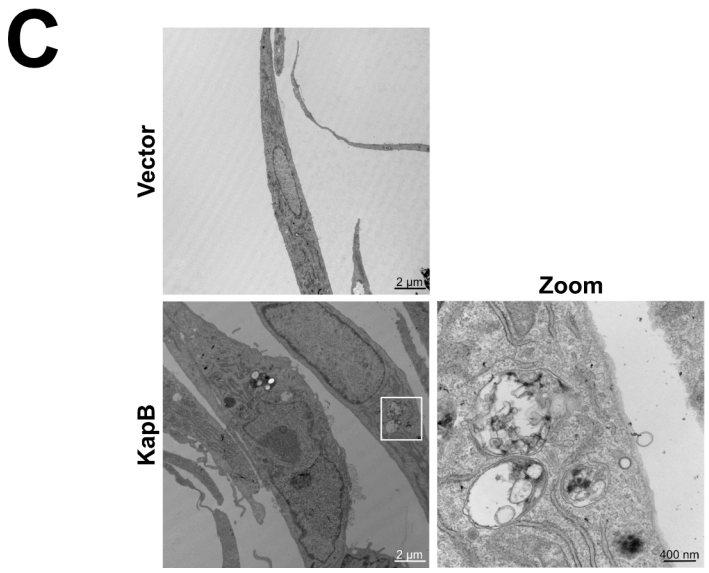
C
Vector
KapB
Zoom
2 µm
2 µm
400 nm

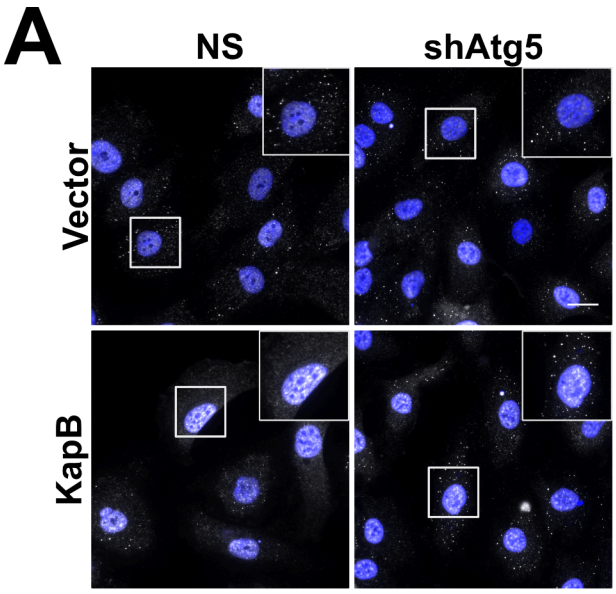
A
NS
shAtg5
Vector
KapB

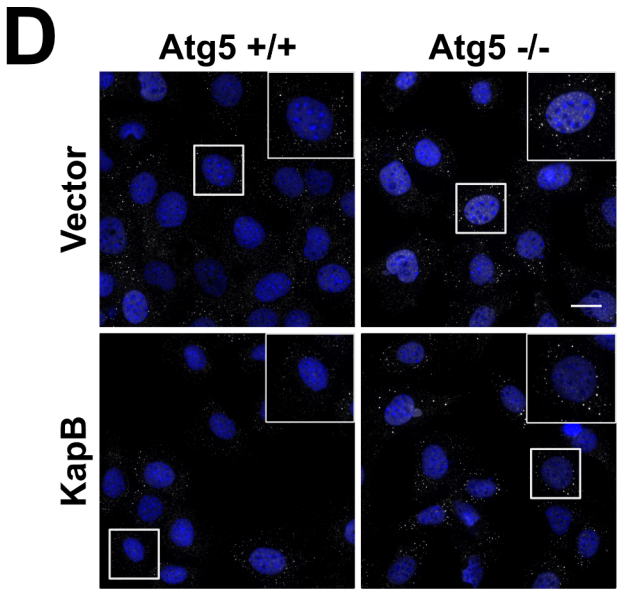
D
Atg5 +/+
Atg5 -/-
Vector
KapB

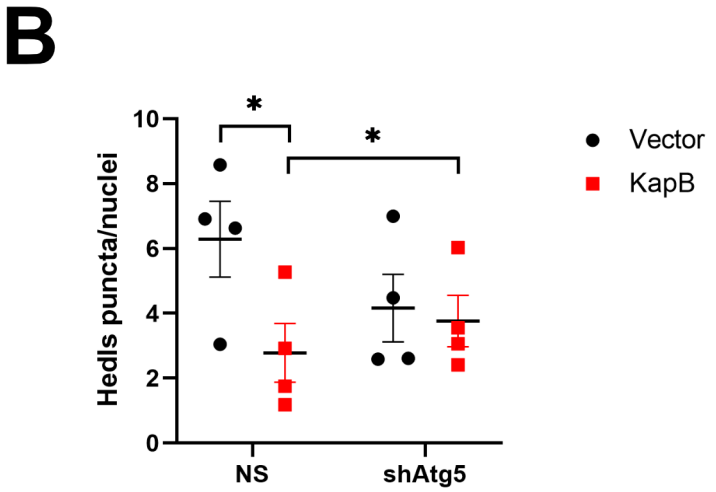
B
Hedls puncta/nuclei
10
8
6
4
2
0
*
*
NS
shAtg5
Vector
KapB

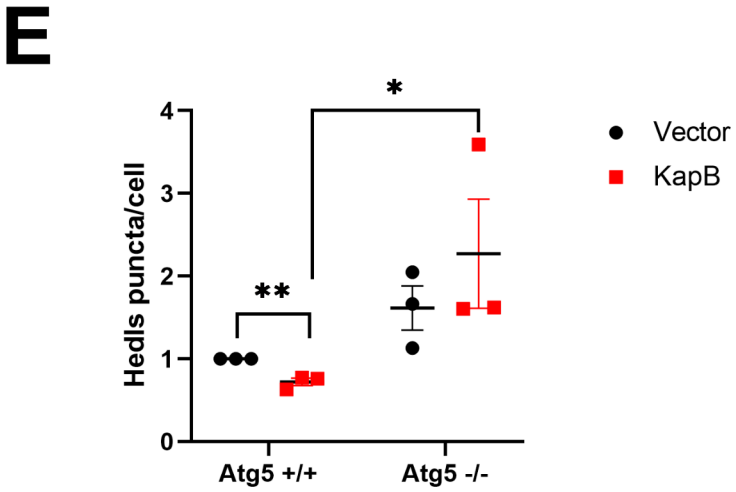
E
Hedls puncta/cell
4
3
2
1
0
*
**
Atg5 +/+
Atg5 -/-
Vector
KapB

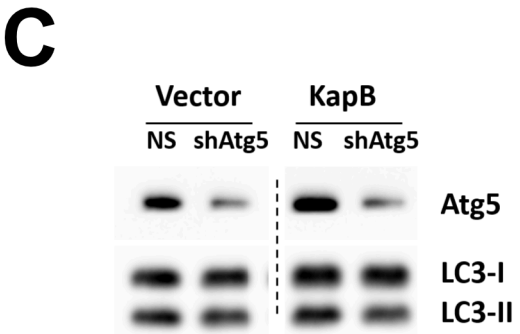
C
Vector
KapB
NS
shAtg5
NS
shAtg5
Atg5
LC3-I
LC3-II

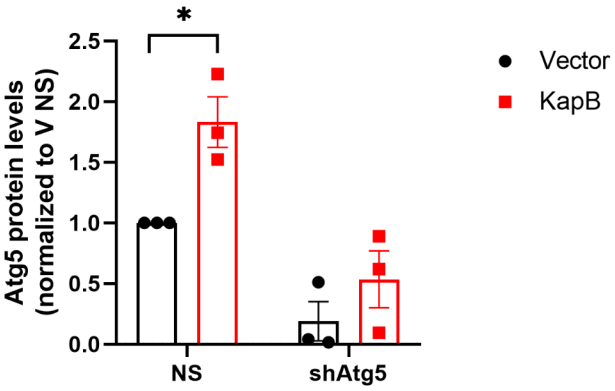
Atg5 protein levels
(normalized to V NS)
2.5
2.0
1.5
1.0
0.5
0.0
*
NS
shAtg5
Vector
KapB

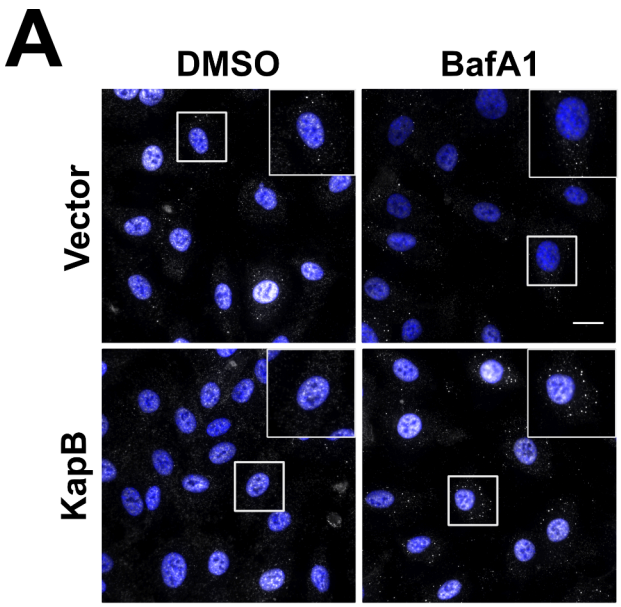
A
DMSO
BafA1
Vector
KapB

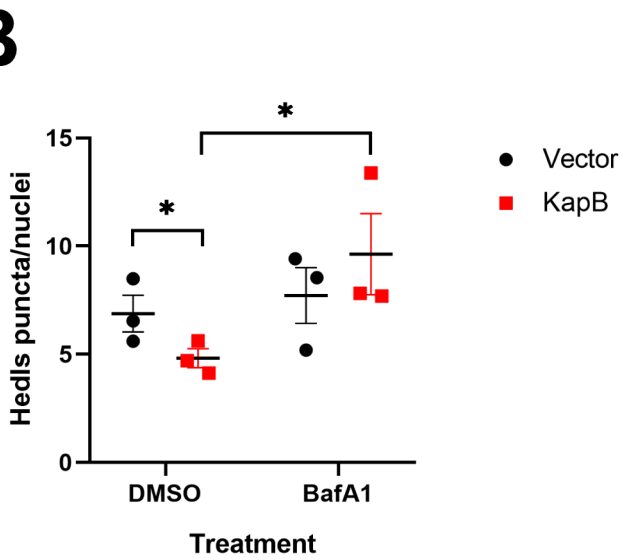
B
Hedls puncta/nuclei
15
10
5
0
*
*
DMSO
BafA1
Treatment
Vector
KapB

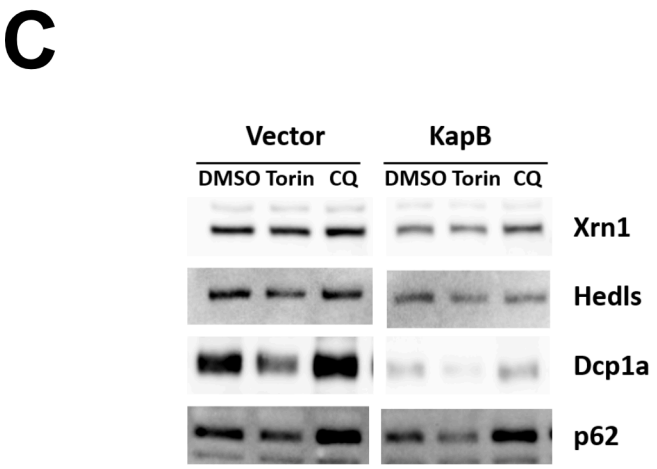
C
Vector
KapB
DMSO Torin CQ
DMSO Torin CQ
Xrn1
Hedls
Dcp1a
p62

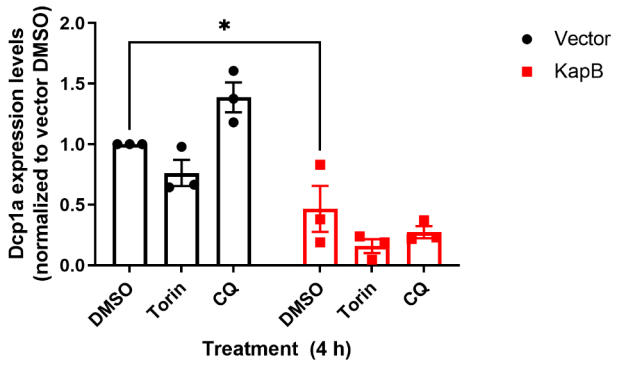
Dcp1a expression levels
(normalized to vector DMSO)
2.0
1.5
1.0
0.5
0.0
*
DMSO
Torin
CQ
DMSO
Torin
CQ
Treatment (4 h)
Vector
KapB

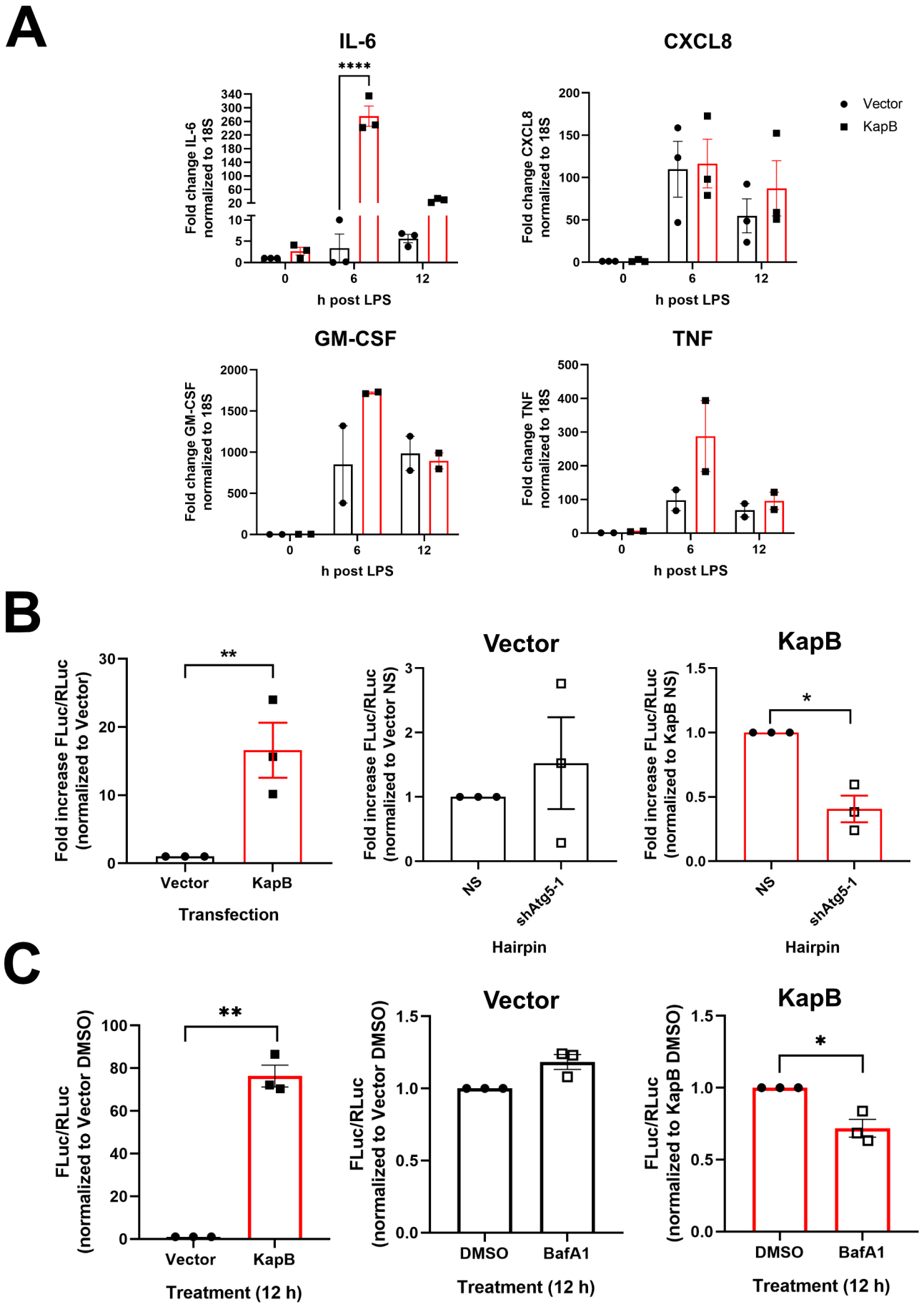
A
IL-6
CXCL8
GM-CSF
TNF
Fold change IL-6 normalized to 18S
Fold change CXCL8 normalized to 18S
Fold change GM-CSF normalized to 18S
Fold change TNF normalized to 18S
h post LPS
****
Vector
KapB
B
Fold increase FLuc/RLuc (normalized to Vector)
Transfection
Vector
KapB
**
Fold increase FLuc/RLuc (normalized to Vector NS)
Fold increase FLuc/RLuc (normalized to KapB NS)
NS
shAtg5-1
Hairpin
*
C
FLuc/RLuc (normalized to Vector DMSO)
FLuc/RLuc (normalized to KapB DMSO)
Treatment (12 h)
DMSO
BafA1

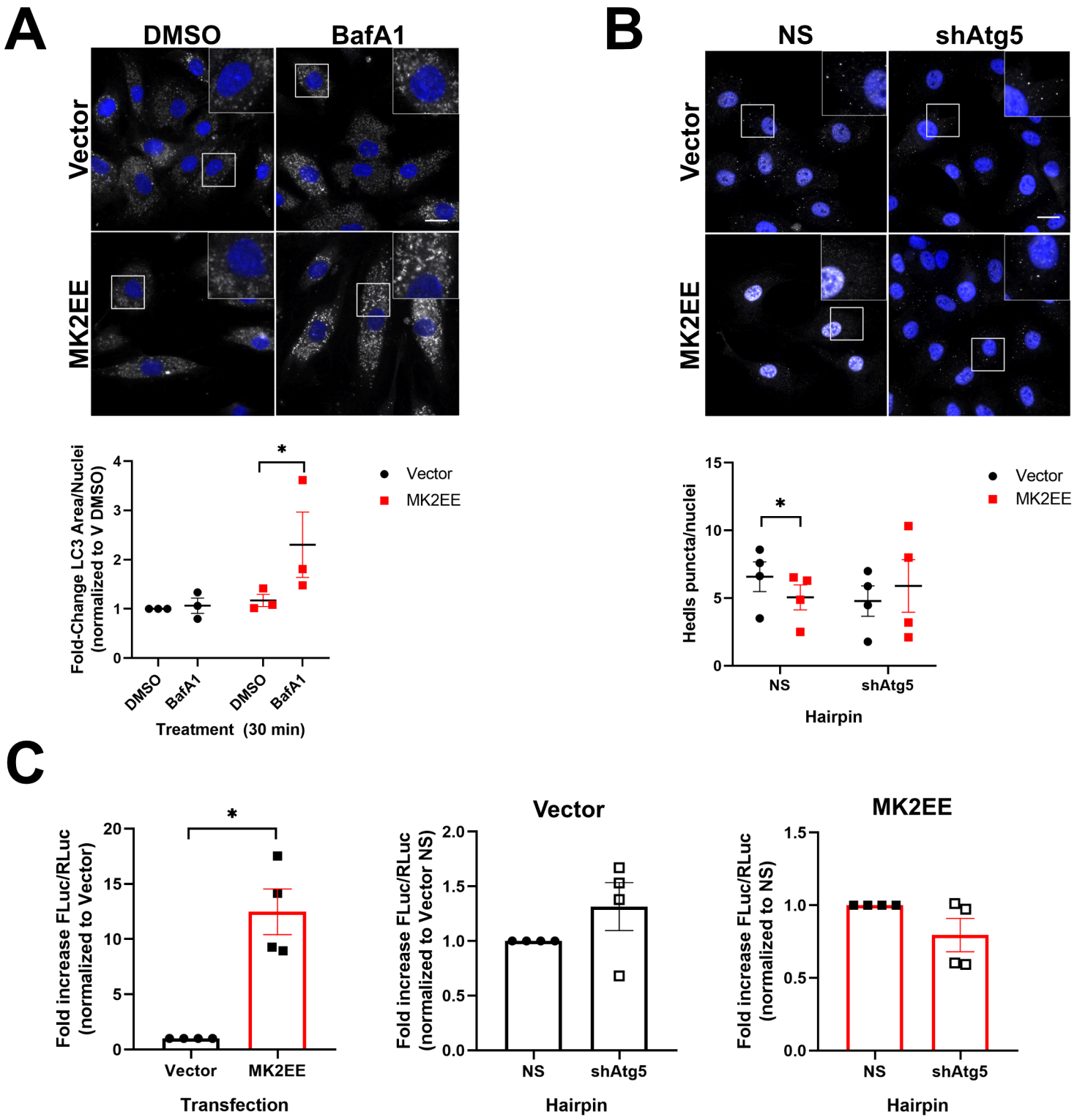
A
DMSO
BafA1
Vector
MK2EE
Fold-Change LC3 Area/Nuclei (normalized to V DMSO)
Treatment (30 min)
DMSO
BafA1
DMSO
BafA1
Vector
MK2EE
B
NS
shAtg5
Vector
MK2EE
Hedls puncta/nuclei
Hairpin
NS
shAtg5
Vector
MK2EE
C
Fold increase FLuc/RLuc (normalized to Vector)
Transfection
Vector
MK2EE
Vector
Fold increase FLuc/RLuc (normalized to Vector NS)
Hairpin
NS
shAtg5
MK2EE
Fold increase FLuc/RLuc (normalized to NS)
Hairpin
NS
shAtg5

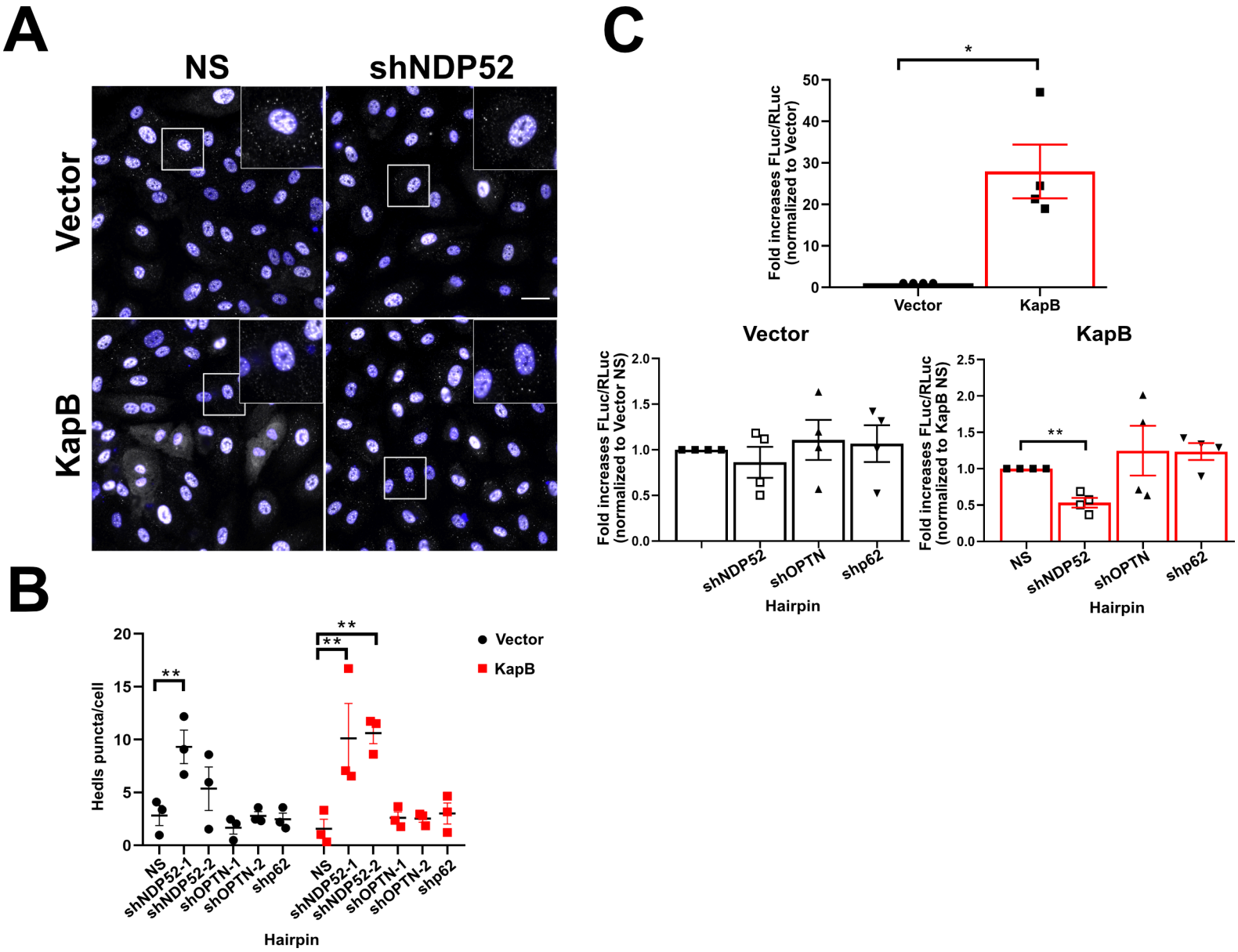
A
NS
shNDP52
Vector
KapB
B
Hedls puncta/cell
Vector
KapB
NS
shNDP52-1
shNDP52-2
shOPTN-1
shOPTN-2
shp62
Hairpin
C
Fold increases FLuc/RLuc (normalized to Vector)
Vector
KapB
Fold increases FLuc/RLuc (normalized to Vector NS)
Fold increases FLuc/RLuc (normalized to KapB NS)
shNDP52
shOPTN
shp62
Hairpin

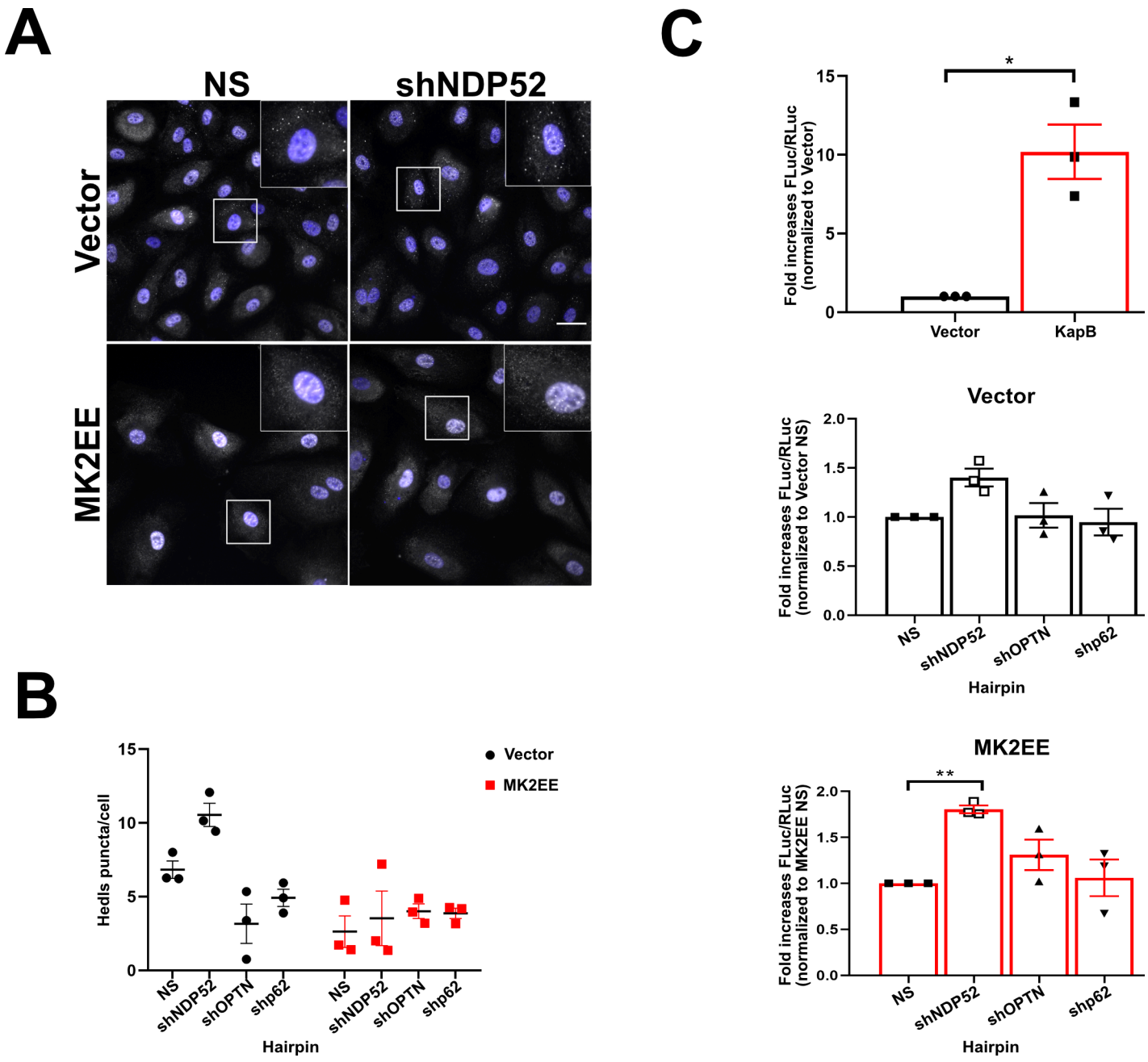
A
NS
shNDP52
Vector
MK2EE
B
Hedls puncta/cell
15
10
5
0
Vector
MK2EE
NS
shNDP52
shOPTN
shp62
NS
shNDP52
shOPTN
shp62
Hairpin
C
Fold increases FLuc/RLuc
(normalized to Vector)
15
10
5
0
*
Vector
KapB
Vector
Fold increases FLuc/RLuc
(normalized to Vector NS)
2.0
1.5
1.0
0.5
0.0
NS
shNDP52
shOPTN
shp62
Hairpin
MK2EE
Fold increases FLuc/RLuc
(normalized to MK2EE NS)
2.0
1.5
1.0
0.5
0.0
**
NS
shNDP52
shOPTN
shp62
Hairpin

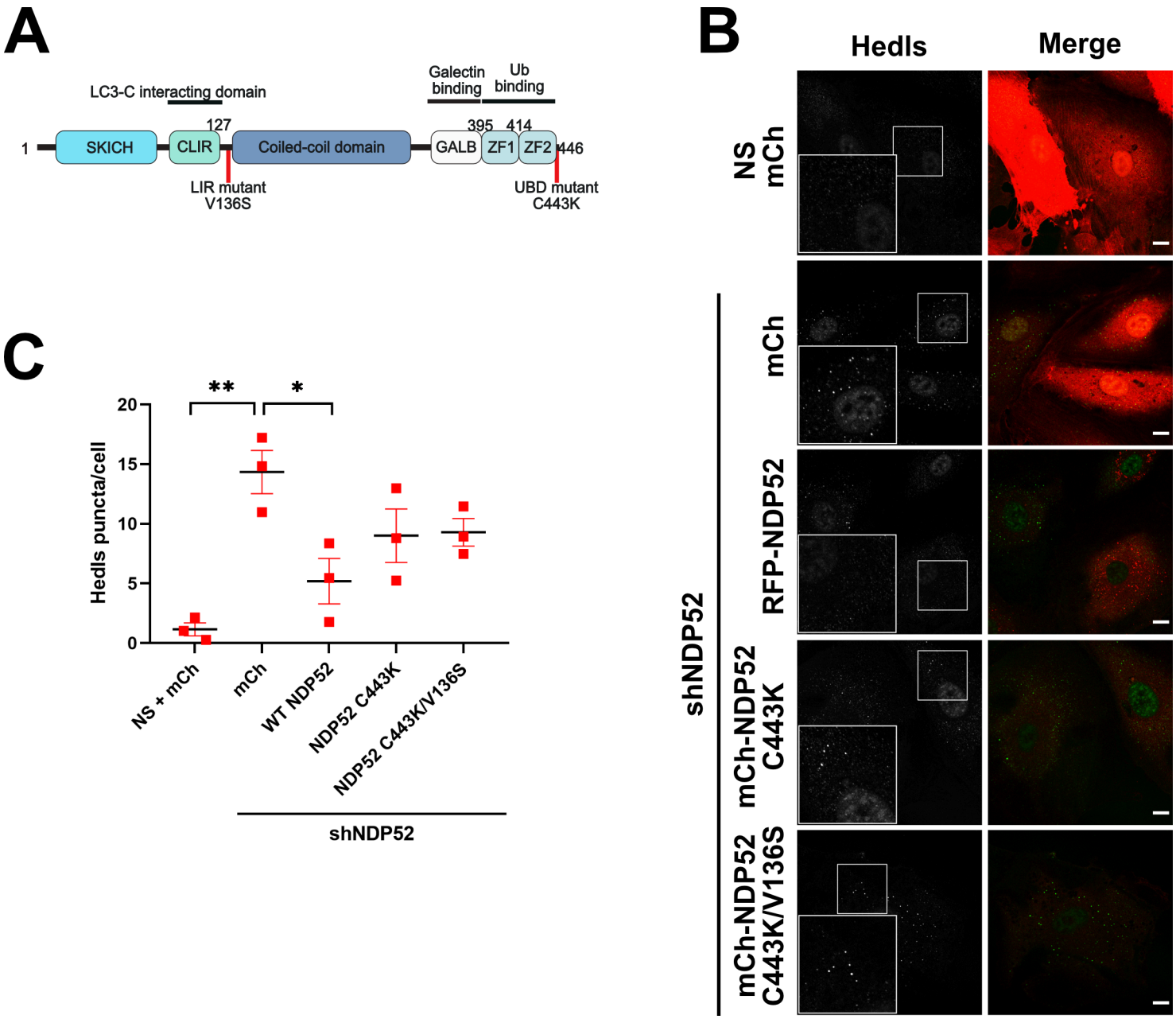
A
LC3-C interacting domain
Galectin binding
Ub binding
1
SKICH
CLIR
127
Coiled-coil domain
GALB
395
ZF1
414
ZF2
446
LIR mutant V136S
UBD mutant C443K
B
HeDls
Merge
NS mCh
mCh
RFP-NDP52
mCh-NDP52 C443K
mCh-NDP52 C443K/V136S
shNDP52
C
HeDls puncta/cell
20
15
10
5
0
**
*
NS + mCh
mCh
WT NDP52
NDP52 C443K
NDP52 C443K/V136S
shNDP52

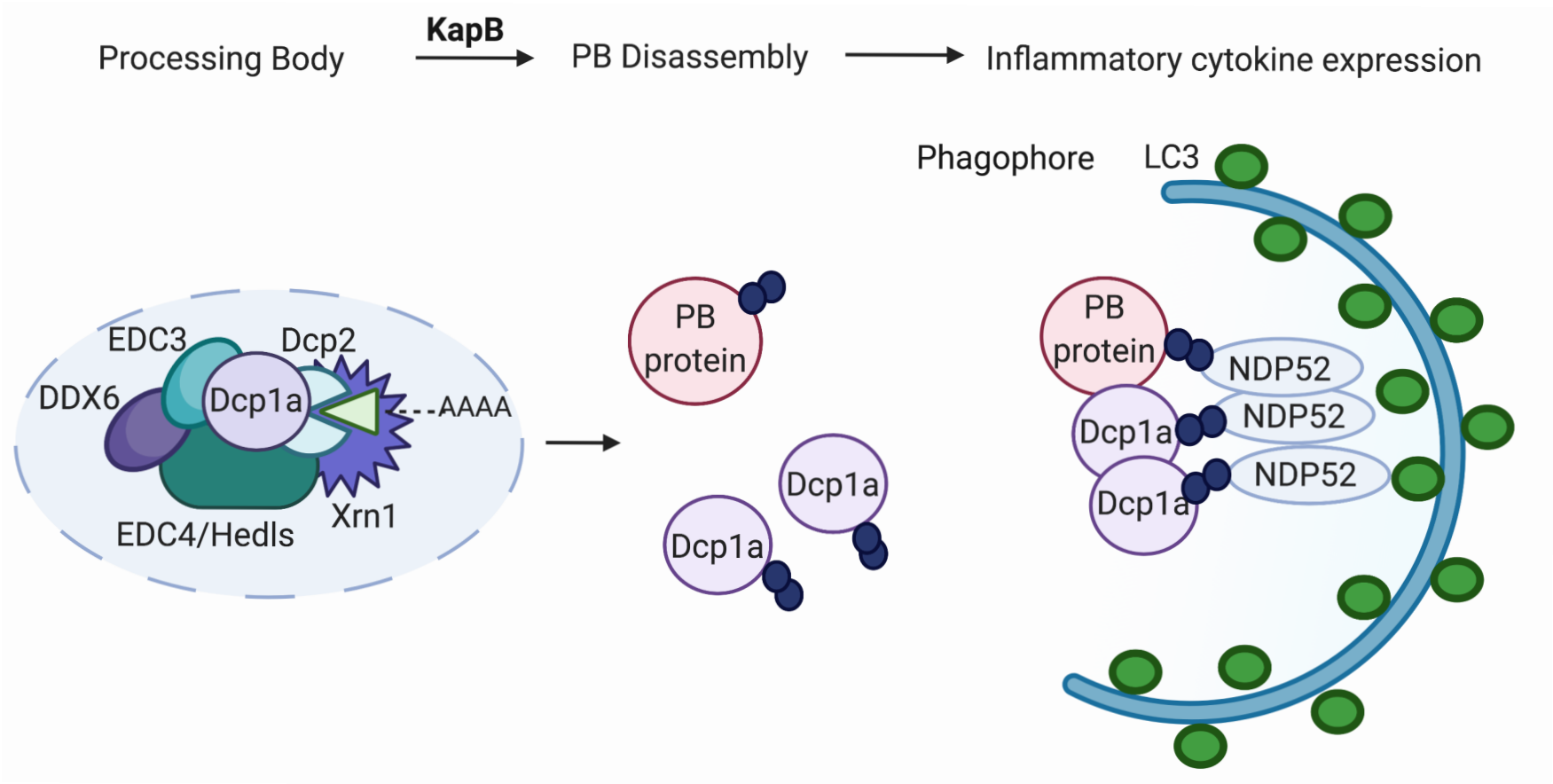
Processing Body
KapB
PB Disassembly
Inflammatory cytokine expression
EDC3
Dcp2
DDX6
Dcp1a
AAAA
Xrn1
EDC4/Hedls
PB protein
Dcp1a
Dcp1a
Phagophore
LC3
PB protein
NDP52
Dcp1a
NDP52
Dcp1a
NDP52

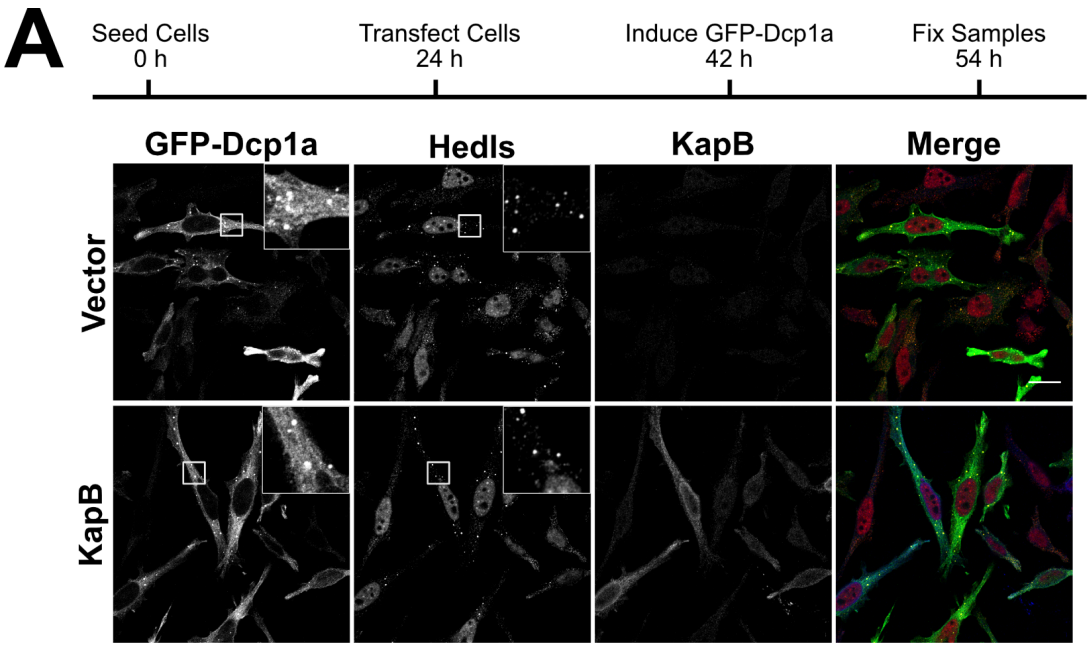
A
Seed Cells
0 h
Transfect Cells
24 h
Induce GFP-Dcp1a
42 h
Fix Samples
54 h
GFP-Dcp1a
Hedls
KapB
Merge
Vector
KapB

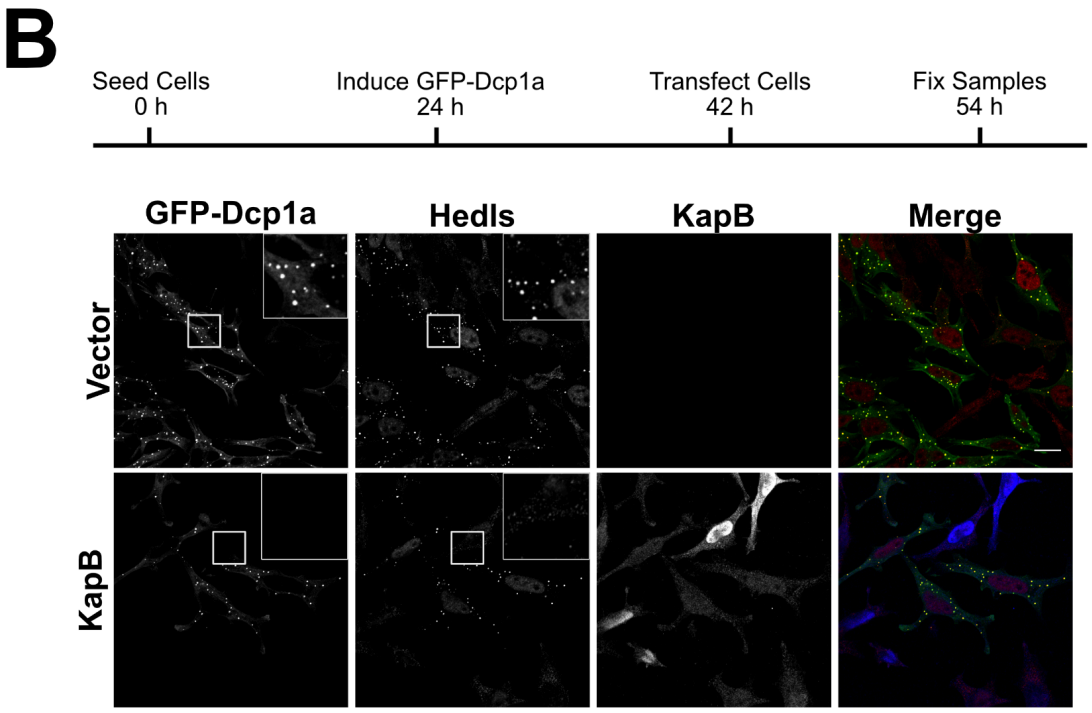
B
Seed Cells
0 h
Induce GFP-Dcp1a
24 h
Transfect Cells
42 h
Fix Samples
54 h
GFP-Dcp1a
Hedls
KapB
Merge
Vector
KapB

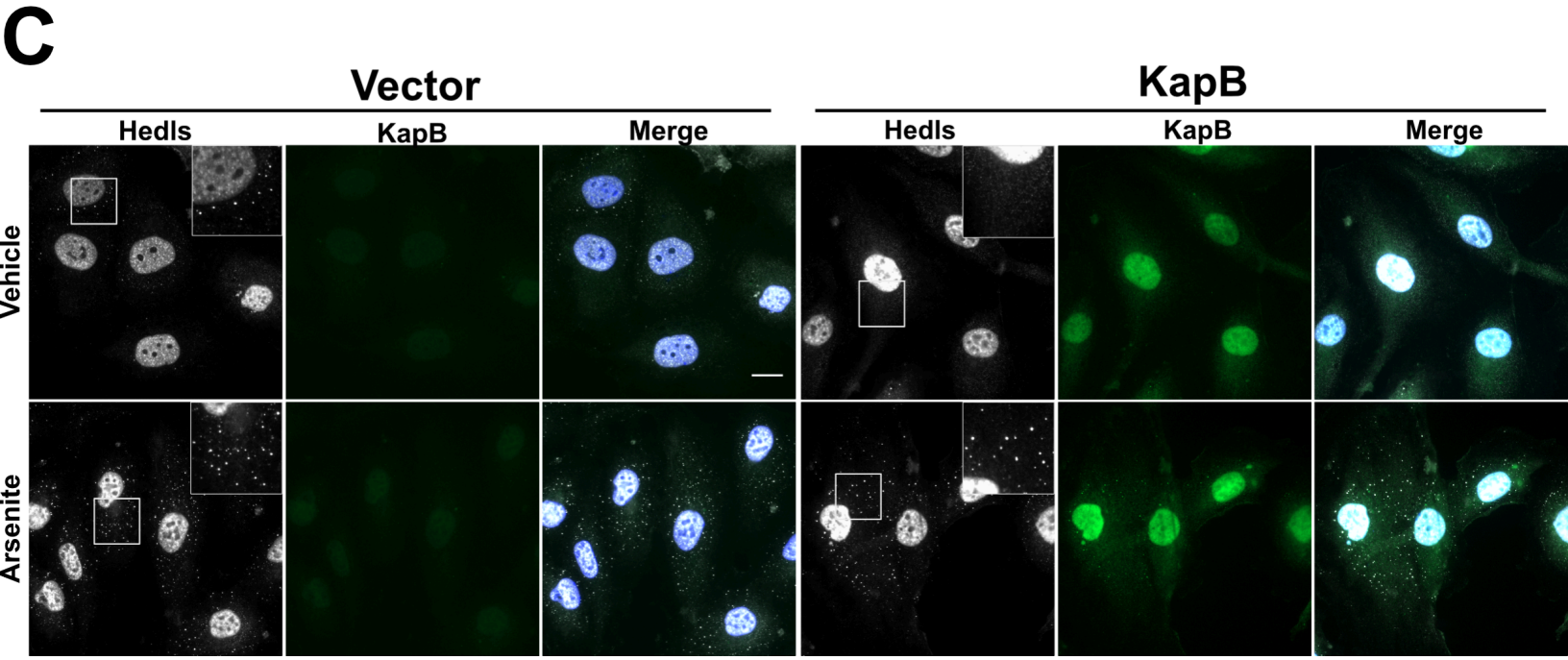
C
Vector
KapB
Hedls
KapB
Merge
Hedls
KapB
Merge
Vehicle
Arsenite

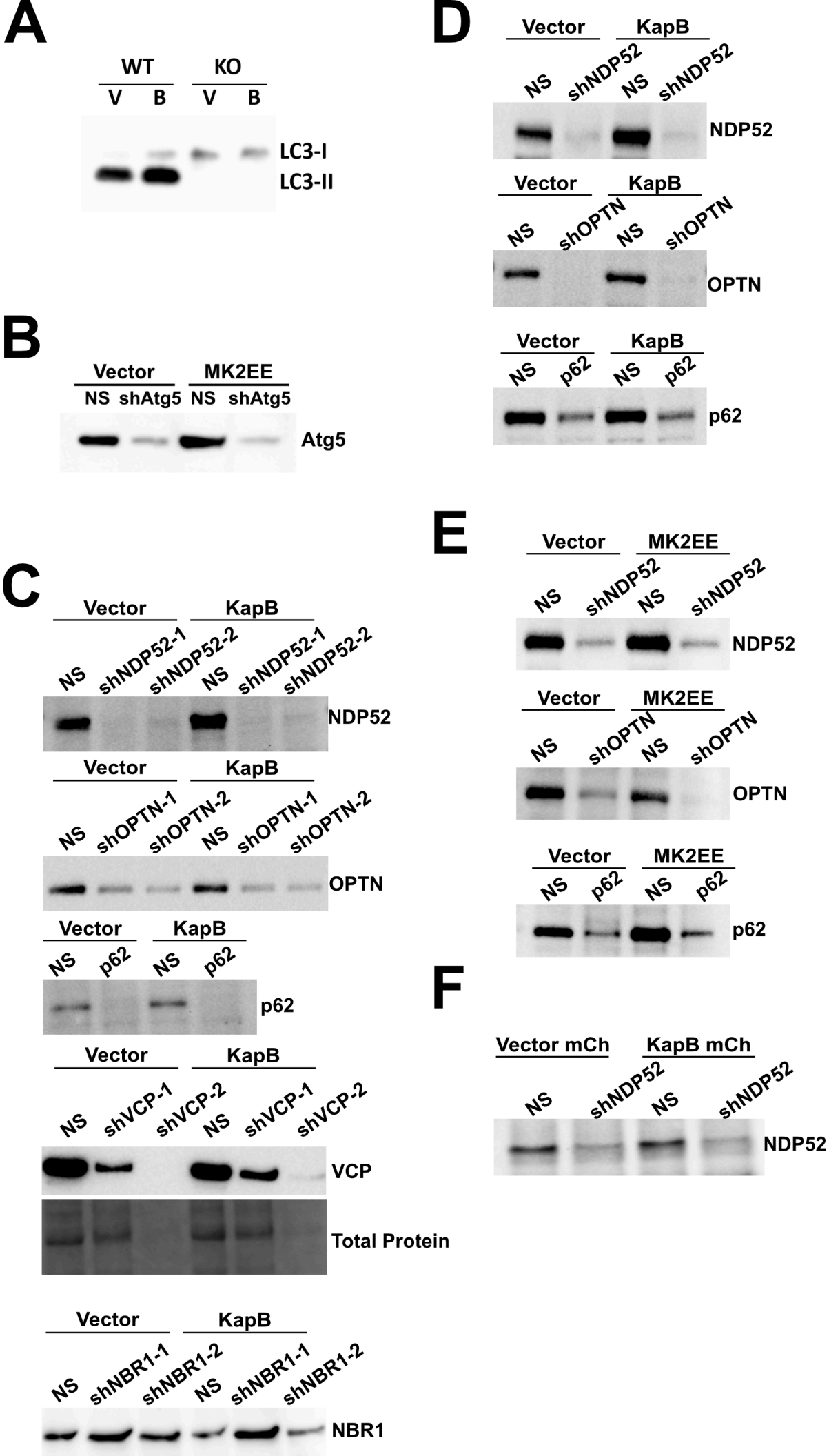
A
WT
KO
V
B
V
B
LC3-I
LC3-II
B
Vector
MK2EE
NS
shAtg5
NS
shAtg5
Atg5
C
Vector
KapB
NS
shNDP52-1
shNDP52-2
NS
shNDP52-1
shNDP52-2
NDP52
Vector
KapB
NS
shOPTN-1
shOPTN-2
NS
shOPTN-1
shOPTN-2
OPTN
Vector
KapB
NS
p62
NS
p62
p62
Vector
KapB
NS
shVCP-1
shVCP-2
NS
shVCP-1
shVCP-2
VCP
Total Protein
Vector
KapB
NS
shNBR1-1
shNBR1-2
NS
shNBR1-1
shNBR1-2
NBR1
D
Vector
KapB
NS
shNDP52
NS
shNDP52
NDP52
Vector
KapB
NS
shOPTN
NS
shOPTN
OPTN
Vector
KapB
NS
p62
NS
p62
p62
E
Vector
MK2EE
NS
shNDP52
NS
shNDP52
NDP52
Vector
MK2EE
NS
shOPTN
NS
shOPTN
OPTN
Vector
MK2EE
NS
p62
NS
p62
p62
F
Vector mCh
KapB mCh
NS
shNDP52
NS
shNDP52
NDP52

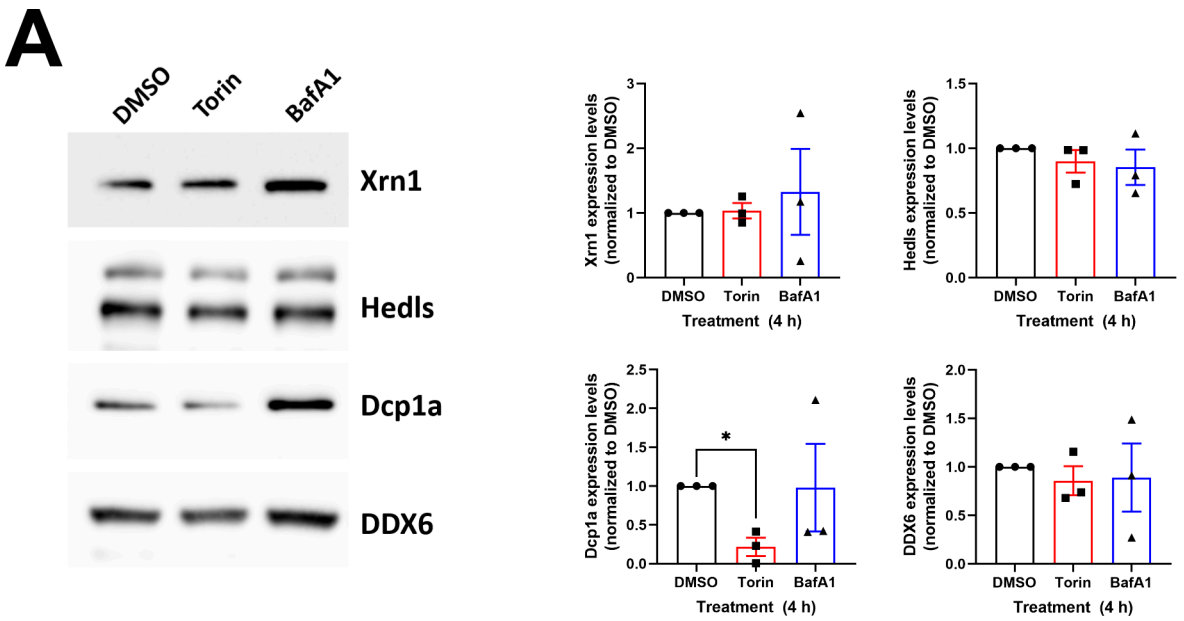
A
DMSO
Torin
BafA1
Xrn1
Hedls
Dcp1a
DDX6
Xrn1 expression levels (normalized to DMSO)
Hedls expression levels (normalized to DMSO)
Dcp1a expression levels (normalized to DMSO)
DDX6 expression levels (normalized to DMSO)
Treatment (4 h)
*

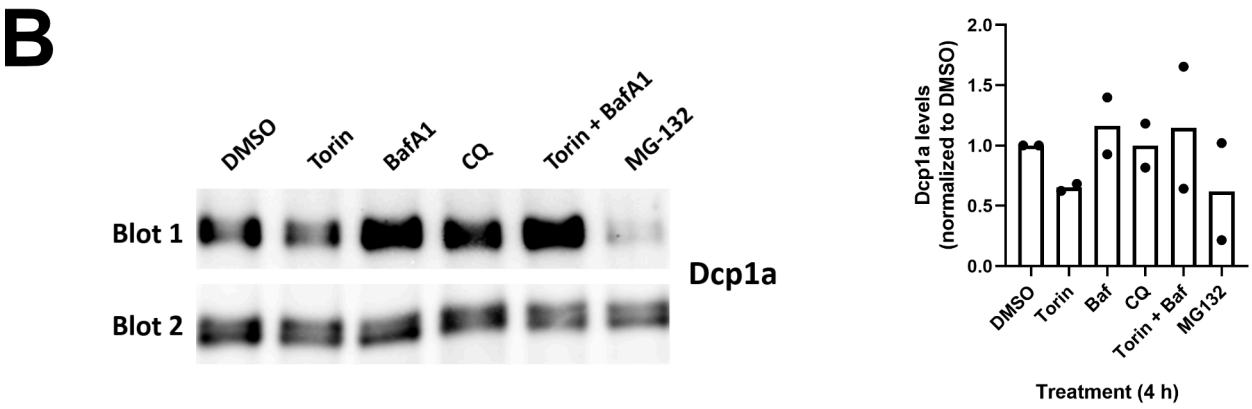
B
DMSO
Torin
BafA1
CQ
Torin + BafA1
MG-132
Blot 1
Blot 2
Dcp1a
Dcp1a levels (normalized to DMSO)
Baf
Torin + Baf
MG132
Treatment (4 h)

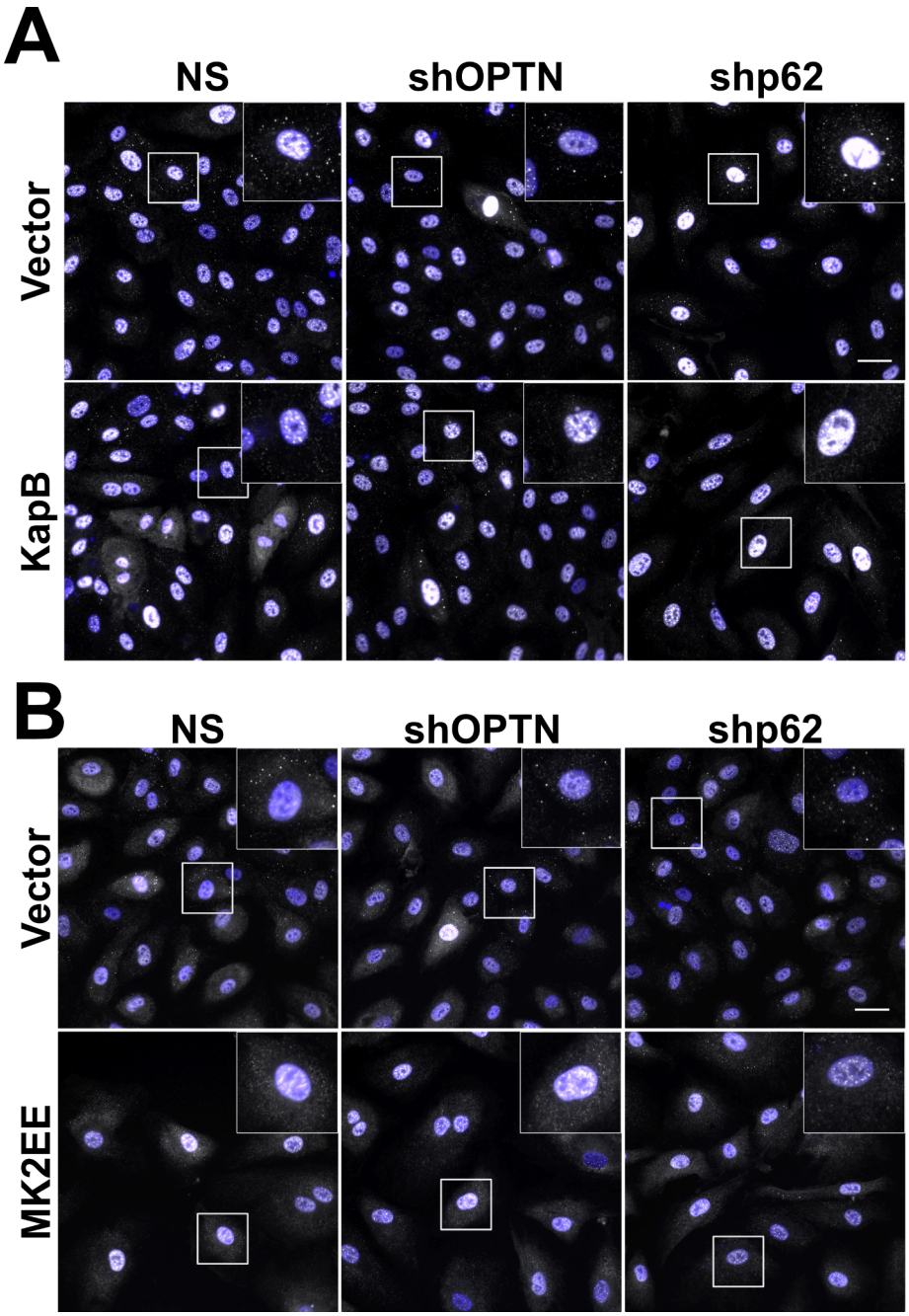
A
NS
shOPTN
shp62
Vector
KapB
B
NS
shOPTN
shp62
Vector
MK2EE

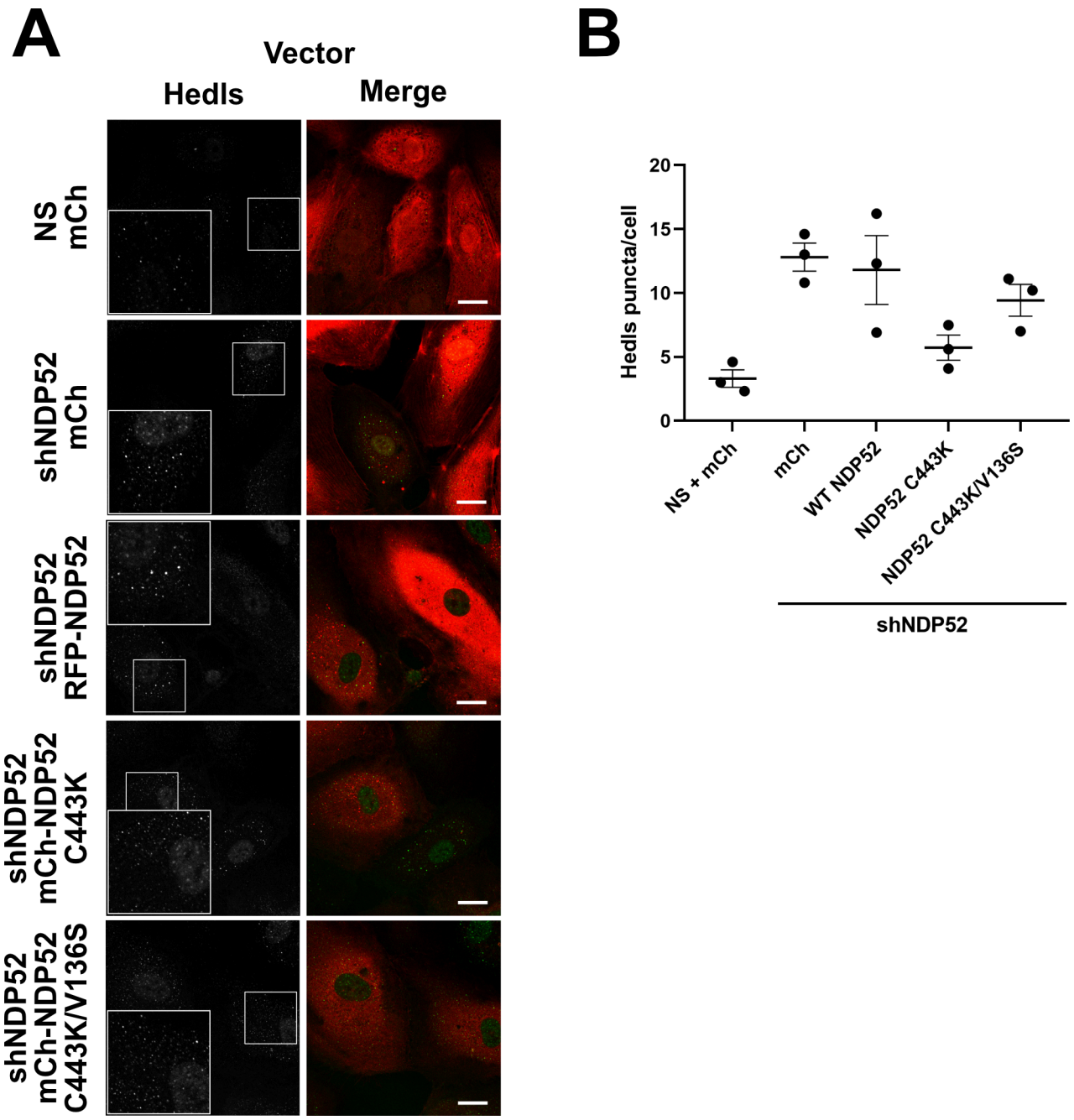
A
Vector
HedIs
Merge
NS mCh
shNDP52 mCh
shNDP52 RFP-NDP52
shNDP52 mCh-NDP52 C443K
shNDP52 mCh-NDP52 C443K/V136S
B
HedIs puncta/cell
20
15
10
5
0
NS + mCh
mCh
WT NDP52
NDP52 C443K
NDP52 C443K/V136S
shNDP52

A

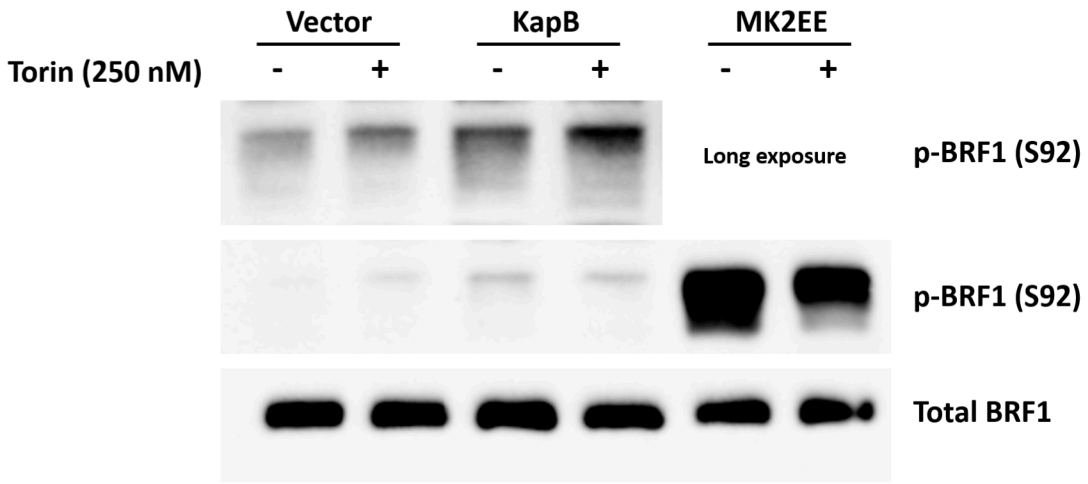
Vector
KapB
MK2EE
Torin (250 nM)
-
+
-
+
-
+
Long exposure
p-BRF1 (S92)
p-BRF1 (S92)
Total BRF1